Density-functional study of the $La_2Zr_2O_7$ low-index surfaces

Yves A. Mantz[a,*], Yuhua Duan[b]

[a] *U.S. Department of Energy, National Energy Technology Laboratory, 3610 Collins Ferry Road, P.O. Box 880, Morgantown, West Virginia 26507, United States*

[b] *U.S. Department of Energy, National Energy Technology Laboratory, 626 Cochrans Mill Road, P.O. Box 10940, Pittsburgh, Pennsylvania 15236, United States*

Abstract

To explain the ability of lanthanum zirconate ($La_2Zr_2O_7$, LZ) and various doped forms of LZ to function as catalysts, an understanding of LZ surface structures is needed. Accordingly, certain LZ surfaces that are expected to be prevalent in prepared samples of LZ, namely, the low-index (001), (011), and (111) surfaces, are examined at the level of density-functional theory. All possible surface terminations of these surfaces formed by cleaving a perfect LZ crystal, termed ideal surface terminations, are considered, as well as several defective surface terminations of a given surface. Surface energies and surface free energies are computed, and surface phase diagrams (SPDs) of the (001), (011), and (111) surfaces are obtained. From these SPDs, the thermodynamically preferred surface termination of the (001), (011), or (111) surface is concluded to be nonideal over a large range of temperature and oxygen gas partial pressure conditions. This finding is unchanged if the SPDs are determined more accurately by taking into account certain vibrational contributions obtained from computed phonon dispersions. In addition to this finding, a way to use results to characterize the surfaces of synthesized LZ crystallites is discussed, but the shapes or dimensions of the crystallites first need to be obtained.

Keywords: $La_2Zr_2O_7$, pyrochlore oxide, surface free energy, density-functional theory

*Corresponding author

Email addresses: yves.mantz@netl.doe.gov (Yves A. Mantz), yuhua.duan@netl.doe.gov (Yuhua Duan)

1. Introduction

Lanthanum zirconate ($La_2Zr_2O_7$, LZ) and doped forms of LZ have been shown to be effective catalysts. In particular, doped forms of LZ can catalyze different reactions to make synthesis gas or syngas, which is a mixture of CO and H_2. These reactions are the partial oxidation of liquid fuel into syngas ($2C_nH_m + nO_2 \rightarrow 2nCO + mH_2$) [1–5], the dry reforming of methane into syngas ($CH_4 + CO_2 \rightarrow 2CO + 2H_2$) [6–14], and the bi-reforming of methane into syngas ($3CH_4 + CO_2 + 2H_2O \rightarrow 4CO + 8H_2$) [15, 16]. In addition, a doped form of LZ is able to catalyze the oxy-reforming of methane into syngas ($3CH_4 + CO_2 + O_2 \rightarrow 4CO + 6H_2$) and is only slowly deactivated during the course of reaction [16]. The conversion of liquid fuel into syngas can be used to operate a solid oxide fuel cell (SOFC) for the auxiliary power unit of a long-haul truck or for remote or distributed power generation. The reactions converting methane into syngas are, in fact, ways to convert methane into high-value products, because syngas can be used to make various chemicals and fuels such as methanol and diesel fuel. Besides these applications of doped forms of LZ as catalysts, LZ and doped forms of LZ can catalyze a process that produces energy directly, namely, the combustion of methane ($CH_4 + 2O_2 \rightarrow CO_2 + 2H_2O$) [17].

Compounds based on LZ have also been examined as catalysts for other processes. In order to convert syngas into higher alcohol products that can be used as fuels or fuel additives or easily transported and converted back into syngas to power a SOFC, a doped form of LZ was tested as a catalyst for higher alcohol synthesis by CO hydrogenation [$nCO + 2nH_2 \rightarrow C_nH_{2n+1}OH + (n-1)H_2O$, $n = 2{-}8$] [18]. However, it was reported to favor methanol formation versus higher alcohols. In addition, the use of a LZ-based compound was considered as a way to improve the performance of SOFCs. In these devices, a fuel such as hydrogen gas and oxygen gas are electrochemically converted into water and electricity at high temperature ($2H_2 + O_2 \rightarrow 2H_2O$). A key step in this process is the reduction of oxygen gas ($O_2 + 4e^- \rightarrow 2O^{2-}$), and a doped form of LZ was tested as a cathode infiltrate, or catalyst deposited atop the cathode, to make this step faster and the fuel cell more efficient [19]. Unfortunately, when the material was deposited, the effect on cell performance was negative.

In certain of the above processes, the tested materials are able to function as catalysts,

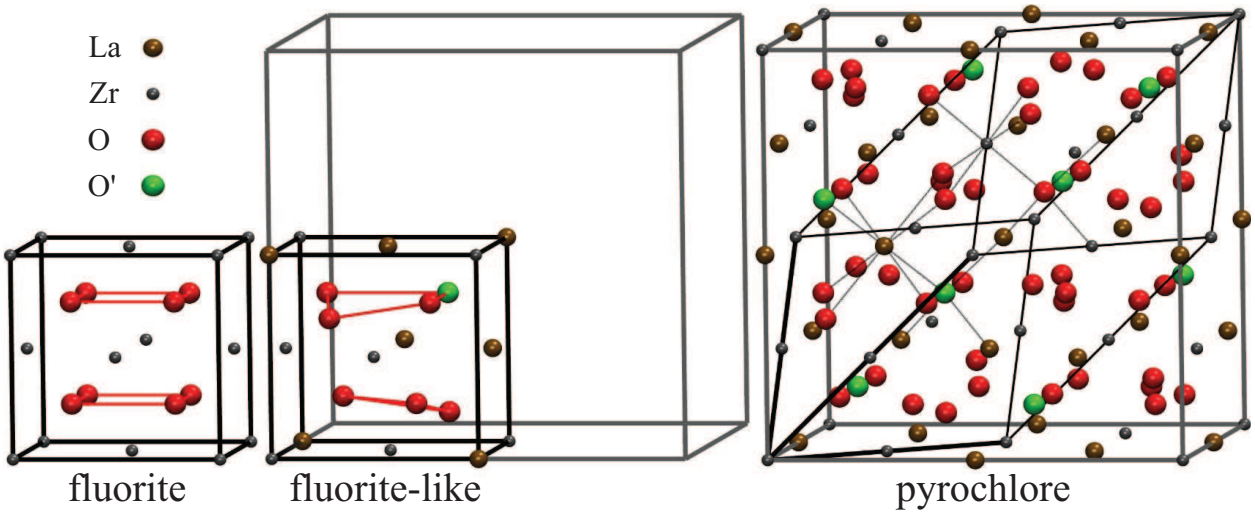

Figure 1: Structure of bulk LZ. The fluorite unit cell of ZrO_2 (left) is modified to form a fluorite-like structural unit (middle), which is the basis for conventional cubic (right, in gray) and primitive triclinic (right, in black) unit cell representations of bulk LZ. In this and other figures, atom types are shown in a key in the figure.

whereas in others, they are not or are not very effective. To help explain these observations and develop better catalysts for the above processes, an understanding of LZ surface structures would be useful.

A good starting point is to examine the structure of bulk LZ. The structure is pyrochlore oxide or pyrochlore, for short [20, 21]. The pyrochlore structure of LZ is derived from the fluorite structure of ZrO_2. A fluorite unit cell of ZrO_2 is shown in Fig. 1, on the left. This unit cell can be modified by removing an oxygen atom and allowing for two different kinds of metal atoms to create a fluorite-like structural unit, Fig. 1, middle. This structural unit and a structural unit related to it by symmetry can then be used to make a $2 \times 2 \times 2$ arrangement of structural units, which is the conventional unit cell of bulk LZ. Conventional and primitive unit cell representations of bulk LZ are shown in gray and black, respectively, Fig. 1, right. In both cells, four different atom types are found, namely, La and Zr atoms and two different types of O atoms, labeled O and O′. The O and O′ atoms are distinguished by different local environments, with O atoms having two La−O and two Zr−O bonds and O′ atoms having four La−O′ bonds. In terms of atom types, one formula unit of LZ is written as $La_2Zr_2O_6O'$. In addition, the number of atoms contained in both cells is large, 88 atoms or eight formula units of LZ in the conventional cell and 22 atoms or two formula

units of LZ in the primitive cell. Due to the large number of atoms and atom types present in both cell representations, the surfaces of LZ are expected to exhibit a rich diversity of structures and compositions. As for other materials, different possible surface terminations of a given surface such as (001) are expected upon cleaving the bulk crystal, where a surface termination is defined as a unique terminating plane or top few terminating planes of atoms.

As for the surfaces of LZ themselves, some information is beginning to emerge. Several experimental syntheses of LZ crystallites [22–26] as well as experimental studies of LZ thin films [27, 28] are available. From this work, an important conclusion is that, in crystalline samples of LZ, the families of planes {100}, {110}, and {111} are likely to be well represented, based on the fact that these families of planes are typically well represented in crystals, the presence of certain peaks in X-ray diffraction spectra of different samples [22–26], and transmission electron microscopy images of square-like particles in a sample [22]. To characterize these different low-index surfaces, only the (001), (011), and (111) surfaces need to be considered, because the conventional unit cell of bulk LZ is cubic. As a follow-up to a couple of preliminary theoretical studies of LZ surfaces [29, 30], the first atomistic-level study of LZ surfaces was recently published, a theoretical study of the LZ (001) and (011) surfaces [31]. In that work, an ideal surface termination is defined as a surface termination that is formed by cleaving the bulk crystal, and the different possible ideal and selected defective surface terminations of the (001) and (011) surfaces are examined. The different surface terminations are relaxed, and surface free energies are computed at the level of density-functional theory (DFT) and used to make surface phase diagrams (SPDs) of the (001) and (011) surfaces. Based on the SPD of the (001) surface and a detailed error analysis, the thermodynamically preferred surface termination of the (001) surface is concluded to be nonideal over a large set of environmental conditions of temperature T and oxygen gas partial pressure p_{O_2}.

The main objectives of the present work are to determine if a structural description similar to that given above for the (001) surface from Ref. [31] can also be given for the (011) and (111) surfaces and if an even larger set of T and p_{O_2} conditions can be identified where the (001) surface may be nonideal. Following Ref. [31], the stabilities of relaxed ideal versus defective surface terminations of a surface are compared. In addition, Wulff shapes, or crystal shapes with minimal surface free energy, are made to be compared to experimental crystal

shapes to draw insight into the surface structures of the experimental shapes. However, the experimental shapes first need to be obtained to permit the comparison.

2. Computational approach

2.1. Levels of density-functional theory and other information

All results are obtained at the level of DFT using, in most cases, the generalized gradient approximation (GGA) and PW91 functional [32, 33], a projector augmented wave (PAW) [34, 35] pseudopotential set [36] that includes a harder oxygen pseudopotential [36, 37], and a plane-wave basis set cutoff of 400 eV. Appropriate Monkhorst−Pack k-point meshes [38] are used for bulk materials and surfaces, for example, $4 \times 4 \times 4$ for bulk LZ and $4 \times 4 \times 1$ for LZ surfaces.

Certain results, namely, vibrational frequencies and phonon density of states (DOS) plots, are obtained at a lower level of theory for computational efficiency. This level of theory is identical to the one described above, except that a softer oxygen pseudopotential [36, 37] and cutoff energy of 250 eV are used.

Additional computations are performed within the local density approximation (LDA) using the CA functional [39] and a PAW pseudopotential set for use with this functional [36], but keeping other technical parameters the same as those at the PW91 level of theory with a 400-eV cutoff energy described above.

To model the surface terminations, the periodic slab technique is used. A slab model plus a vacuum region of at least 16 Å are periodically replicated in all three dimensions.

Lastly, different types of computations are performed, such as geometry optimizations to obtain minimum-energy structures and phonon DOS computations, using the Vienna ab initio simulation package (VASP) [40–43] and the PHONON software package [44]. Molecular models are built using Materials Studio [45], structures are drawn using VMD [46], and Wulff shapes are constructed using an on-line software program [47].

2.2. Surface models and other computational details

In this work, all possible ideal and selective defective surface terminations of a surface are examined. The number of different possible ideal LZ (001), (011), and (111) surface

terminations is four, four, and eight, respectively. These surface terminations are formed by cleaving the bulk crystal to expose different atomic planes. Some of these planes are identical. Thus, an ideal surface termination of the (001), (011), or (111) surface is uniquely defined by specifying the top 1−3 layers of atoms. Another description of the ideal surface terminations can also be given that is more revealing. Specifically, an ideal (001), (011), or (111) surface termination is described by a top layer or multilayer of atoms that is paired with a complementary layer or multilayer of atoms to form a structural unit that is repeated throughout the crystal. Each of the ideal surface terminations is polar: assigning formal ionic charges to atoms of +3 (La), +4 (Zr), and −2 (O and O′), the top layer or multilayer of atoms is always charged, while the complementary layer or multilayer of atoms is always oppositely charged. Thus, the repeat unit is polarized. For example, a (001) surface can be formed that is terminated by O_4O' per surface unit cell. This terminating layer is designated L3, with a charge of $-10e$ assuming formal ionic charges for atoms. The underlying three atomic layers are O−La_2Zr_2−O, and this multilayer of atoms is denoted L4, with a formal charge of $+10e$. The rest of the crystal is described by alternating L3 and L4 units, forming the structure L3−L4−L3−L4−... . The L3- and L4-terminated surfaces are shown in Fig. 2. The different ideal surface terminations are specified by their terminating layers and multilayer of atoms Lp, p = 1−16, which are defined for the smallest possible surface unit cells in Fig. 2. The complementary units of Lp are Lq, where $q = p + 1$ (p odd) or $p - 1$ (p even). In this work, ideal surface terminations are designated using the letter "c". The L1−L4-terminated surfaces are designated (001) c1−c4, respectively, L5−L8-terminated as (011) c1−c4, respectively, and L9−L16-terminated as (111) c1−c8, respectively.

In addition to ideal surface terminations, several defective surface terminations are also examined. The number of defective (001), (011), and (111) surface terminations examined is 10, 12, and 7, respectively. A defective surface termination is formed by adding one or two oxygen atoms or an O_2 molecule to, or by removing one or more atoms from, an ideal surface termination. More details are given below. Defective surface terminations are designated using the letter "n", for example, the (001) n2 surface.

In total, 45 different surface terminations are examined in this work. They are modeled using symmetric slab models. A symmetric slab model is defined by equivalent surface

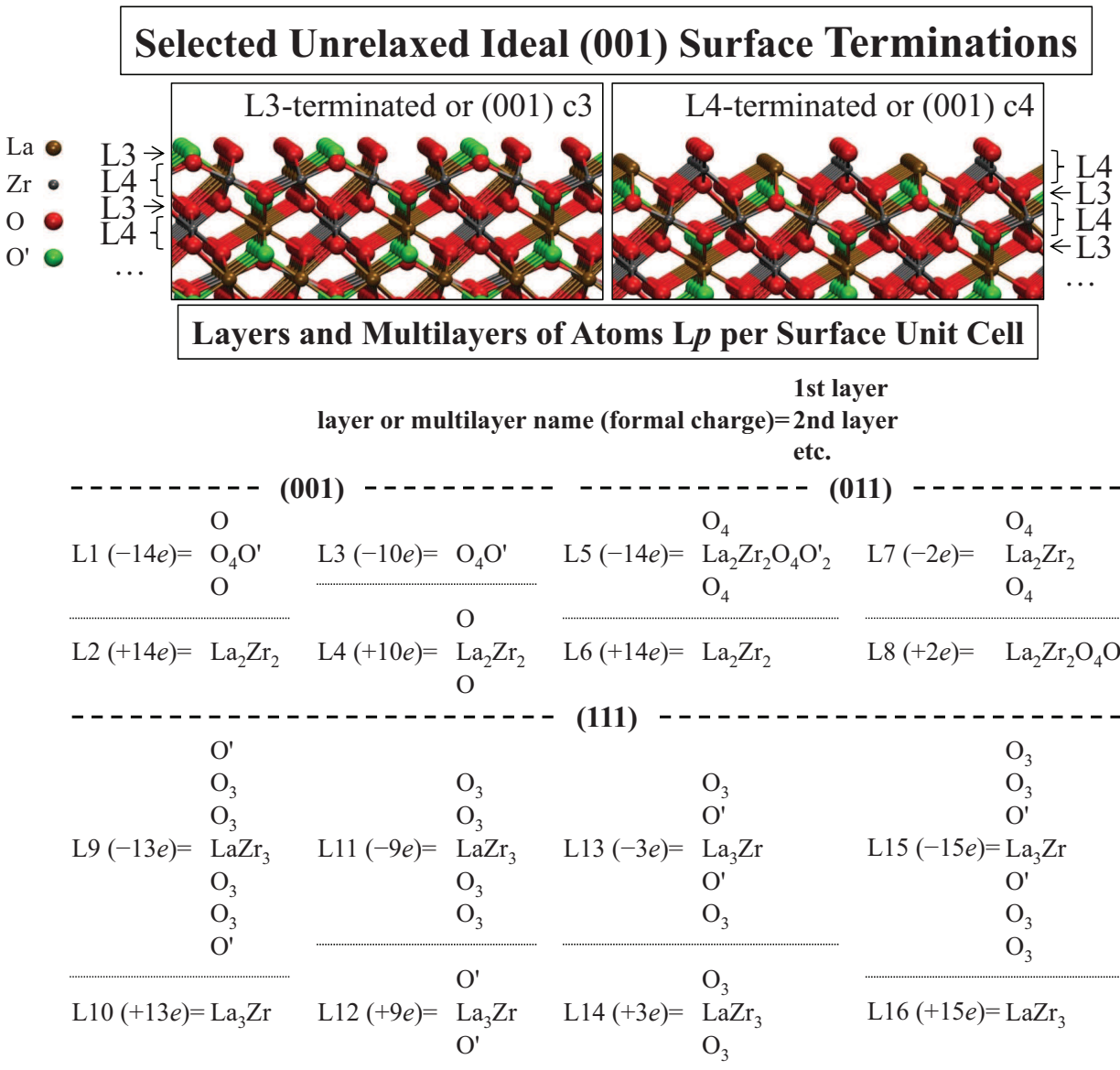

Figure 2: Selected ideal surface terminations of LZ (side views) and definitions of the layers and multilayers of atoms L1−L16.

terminations on the top and bottom of the slab that can be mapped into each other by a symmetry operator such as a mirror plane. Thus, the dipole moment perpendicular to the surface is zero. One symmetric slab model is used to represent every surface termination. The ideal and most defective surface terminations of LZ examined in this work are polar. Thus, the use of symmetric slab models, which are nonpolar, to model them needs to be justified. In a previous theoretical study of the LZ (001) and (011) surfaces, sufficiently thick asymmetric and symmetric slab models are shown to give similar surface energies [31],

justifying the use of the latter type of model in this work.

To complete the description of the surface terminations and models given above, several more details are provided. The surface models of the ideal surface terminations are given by Lp−Lq−Lp−Lq−...−Lp and are quite thick, with either close to or more than 100 atoms each, to ensure a sufficiently large bulk region. However, having the smallest possible surface unit cells, they can still be described as computationally efficient. These cells are a square cell with an edge of length $a_{\mathrm{eq}}/\sqrt{2}$ for (001) surface terminations, a rectangular cell with dimensions of $a_{\mathrm{eq}} \times a_{\mathrm{eq}}/\sqrt{2}$ for (011) surface terminations, and a rhombic cell with a 60° angle and an edge of $a_{\mathrm{eq}}/\sqrt{2}$ for (111) surface terminations, where a_{eq} is the lattice constant of bulk LZ. The value of a_{eq} is obtained from Murnaghan equation of state computations and is set equal to 10.89 Å. The ideal (111) c1 surface is modeled using a different starting structure than that formed by cleaving bulk LZ. This structure is chosen by relaxing several structures in which the positions of the four dangling oxygen atoms singly coordinated to metal atoms are adjusted to form two −O−O− groups and then identifying the most stable relaxed structure and its initial structure, shown in Fig. 3, second row, far left. The models of defective surface terminations are formed by modifying the models Lp−Lq−Lp−Lq−...−Lp of ideal surface terminations as shown in Fig. 3. In a previous theoretical study, the (001) c1−c4, (011) c1−c4, (001) n1 and n2, and (011) n1 and n2 surfaces are examined [31]. Energies and relaxed structures of slab models are obtained at the spin-restricted level, despite the fact that the slab models of the (111) surface terminations are characterized by an odd number of electrons. However, upon reoptimizing slab models of various (111) surface terminations at the spin-unrestricted level, their energies are minimally changed, and surface free energies are not significantly affected. One of the surfaces tested is the (111) n5 surface, which is the only (111) surface termination with an adsorbed O_2 molecule. The surface free energy of this surface termination would be less affected if the O_2 adsorbate were more like a closed-shell peroxide (O_2^{2-}) ion than an O_2 molecule. In fact, the O_2 species, forming multiple bonds with the surface, is predicted to be stretched at spin-restricted and -unrestricted levels of theory and, thus, resemble an O_2^{2-} ion.

In addition to the information given above, other computational details are also relevant to this work. In particular, a careful procedure is used to obtain final relaxed surface ter-

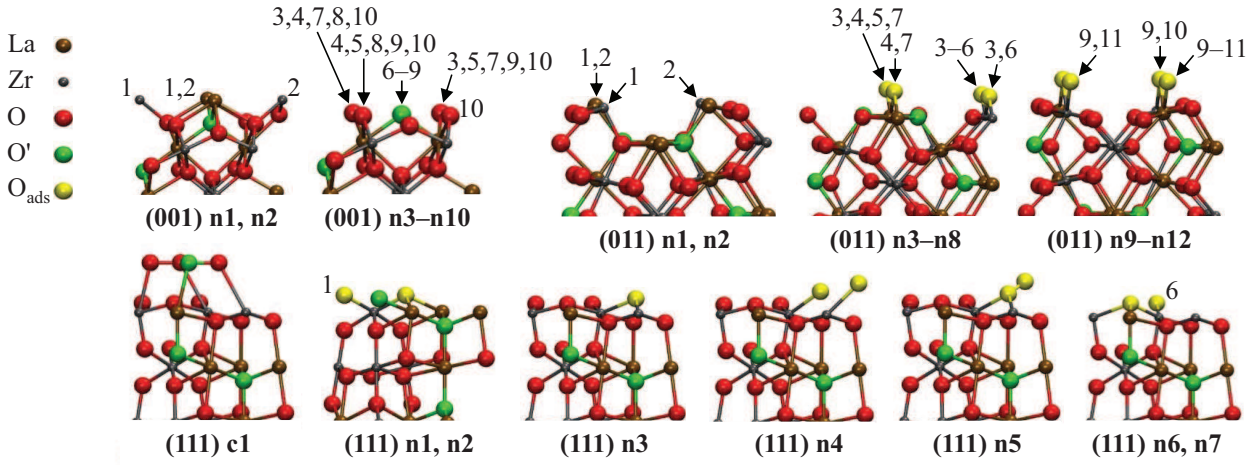

Figure 3: Initial structures of the ideal (111) c1 and defective surface terminations. They are represented as models viewed from the side with 1×1 surface unit cells and several atomic layers shown. In this and other figures, oxygen atoms added to surfaces are denoted O_{ads} in the key, and the O_2 molecule is represented using O_{ads} atoms. The initial structure of the (111) c1 surface is shown in the second row, on the far left. A defective surface termination is formed from the model above its name by removing all atoms with the same number as the defective surface termination. If that number is not assigned to any atoms, then no atoms are removed. An atom with more than one number is removed for all surface terminations with those numbers. For example, the (001) n1 and n2 surfaces are formed from the model labeled "(001) n1, n2" by removing the atoms labeled "1" and "2", respectively.

minations that includes a search for more stable minima using different starting structures. Computations of the O_2 molecule and bulk materials, further description of the defective surface terminations, the procedure to form initial structures of the defective (111) surface terminations, the procedure referred to above to obtain final relaxed surface terminations, further discussion of the (001) n1 and n2 and (011) n1 and n2 surfaces, and computations to obtain vibrational frequencies and phonon DOSs are described in the supplementary material, Section S.1.

2.3. Surface energies

The surface energy E_s is the energy required to form a surface from the bulk crystal. In this work, two equations are used to obtain E_s. They are taken directly from Ref. [31]. For a symmetric slab model having an integer number of formula units,

$$E_{\mathrm{s}} = \frac{1}{2A}(E_{\mathrm{slab}} - nE_{\mathrm{LZ}}^{\mathrm{bulk}}) \tag{1}$$

where E_{slab} is the energy of the slab model (obtained directly from DFT), $E_{\mathrm{LZ}}^{\mathrm{bulk}}$ is the energy of relaxed bulk LZ per formula unit (obtained directly from DFT), the area of one side of the slab is A, and the number of formula units is n. Depending on whether the slab is unrelaxed or relaxed, E_{s} is changed to E_{su} or E_{sr} to denote the unrelaxed or relaxed surface energy, respectively.

For two symmetric slab models, if the sum of formula units in the two models is an integer, an average surface energy can be computed as

$$E_{\mathrm{s}} = \frac{1}{4A}(E_{\mathrm{slab},1} + E_{\mathrm{slab},2} - nE_{\mathrm{LZ}}^{\mathrm{bulk}}) \tag{2}$$

where $E_{\mathrm{slab},1}$ and $E_{\mathrm{slab},2}$ are the energies of the slab models (obtained directly from DFT). As above, either E_{su} or E_{sr} can be obtained. For two symmetric slab models with complementary surface terminations of Lp and Lq, the sum of formula units is always an integer.

2.4. Surface free energies

The surface free energy Ω is the energy required to form a surface from the bulk crystal as a function of environmental conditions. A derivation of an expression for Ω of a LZ surface is given in Ref. [31] that can be followed to derive the expression for Ω that is used in this work. The result is an expression for Ω of a LZ surface that is in thermodynamic equilibrium with separate reference phases for each element. It is a linear function of two variables,

$$\Omega = \frac{1}{A}(\phi_{\mathrm{Zr}} - \Gamma_{\mathrm{Zr,O}}\Delta\mu_{\mathrm{O}} - \Gamma_{\mathrm{Zr,La}}\Delta\mu_{\mathrm{La}}) \tag{3}$$

where the variables $\Delta\mu_{\mathrm{O}}$ and $\Delta\mu_{\mathrm{La}}$ are given by

$$\Delta\mu_{\mathrm{O}} = \mu_{\mathrm{O}} - \frac{1}{2}E_{\mathrm{O_2}}^{\mathrm{gas}} \tag{4}$$

$$\Delta\mu_{\mathrm{La}} = \mu_{\mathrm{La}} - E_{\mathrm{La}}^{\mathrm{bulk}} \tag{5}$$

and ϕ_{Zr}, $\Gamma_{\mathrm{Zr,O}}$, and $\Gamma_{\mathrm{Zr,La}}$ are constants that depend on the surface,

$$\phi_{\mathrm{Zr}} = \frac{1}{2}(E_{\mathrm{slab}} - \frac{N_{\mathrm{Zr}}}{N_{\mathrm{Zr}}^{\mathrm{bulk}}} E_{\mathrm{LZ}}^{\mathrm{bulk}}) - \frac{1}{2}\Gamma_{\mathrm{Zr,O}} E_{\mathrm{O_2}}^{\mathrm{gas}} - \Gamma_{\mathrm{Zr,La}} E_{\mathrm{La}}^{\mathrm{bulk}} \tag{6}$$

$$\Gamma_{\mathrm{Zr},a} = \frac{1}{2}(N_a - N_{\mathrm{Zr}} \frac{N_a^{\mathrm{bulk}}}{N_{\mathrm{Zr}}^{\mathrm{bulk}}}) \tag{7}$$

In the above equations, μ_a are the chemical potentials of the elements a in the slab model, $E_{\mathrm{O_2}}^{\mathrm{gas}}$ is the energy of a relaxed O_2 molecule (obtained directly from DFT), $E_{\mathrm{La}}^{\mathrm{bulk}}$ is the energy of relaxed bulk La per formula unit (obtained directly from DFT) and N_X and N_X^{bulk} are the numbers of atoms of elements X in the slab model and per LZ formula unit, respectively. The variables a = La and O and X = La, Zr, and O. Only relaxed slab models are used to compute Ω.

The $\Gamma_{\mathrm{Zr},a}$ given above are the numbers of excess atoms of a with respect to the number of Zr atoms per side of the slab. For example, a surplus or deficiency of O atoms with respect to the number of Zr atoms in the slab is indicated by a positive or negative $\Gamma_{\mathrm{Zr,O}}$, respectively.

As discussed in Ref. [31], the variable $\Delta\mu_{\mathrm{O}}$ can be related directly to conditions of T and $p_{\mathrm{O_2}}$ using

$$\Delta\mu_{\mathrm{O}} = \frac{1}{2}[G_{\mathrm{O_2}}^{\mathrm{gas}}(T, p_{\mathrm{O_2}}^{\circ}) - G_{\mathrm{O_2}}^{\mathrm{gas}}(T^{\circ}, p_{\mathrm{O_2}}^{\circ}) + k_{\mathrm{B}} T \ln(\frac{p_{\mathrm{O_2}}}{p_{\mathrm{O_2}}^{\circ}})] + \delta\mu_{\mathrm{O}}^{\circ} \tag{8}$$

where $G_{\mathrm{O_2}}^{\mathrm{gas}}(T, p_{\mathrm{O_2}}^{\circ})$ is the experimental free energy of oxygen gas at $T \geq 100$ K and $p_{\mathrm{O_2}}^{\circ}$ and is expressed as a polynomial function in Ref. [31], Supporting Information, Section S5. Also, $T^{\circ} = 298.15$ K, $p_{\mathrm{O_2}}^{\circ} = 1$ atm, and k_{B} is Boltzmann's constant. The constant $\delta\mu_{\mathrm{O}}^{\circ}$ is determined from the standard enthalpy and entropy of oxygen gas, $h_{\mathrm{O_2}}^{\circ}$ and $S_{\mathrm{O_2}}^{\circ}$, respectively:

$$\delta\mu_{\mathrm{O}}^{\circ} = \frac{1}{2}(h_{\mathrm{O_2}}^{\circ} - T^{\circ} S_{\mathrm{O_2}}^{\circ}) - \frac{1}{2} E_{\mathrm{O_2}}^{\mathrm{gas}} = \frac{1}{2} \sum_{M_x\mathrm{O}_y} [\frac{1}{y}(E_{M_x\mathrm{O}_y}^{\mathrm{bulk}} - x E_M^{\mathrm{bulk}} - \Delta H_{\mathrm{f},M_x\mathrm{O}_y}^{\circ})] - \frac{1}{2}(T^{\circ} S_{\mathrm{O_2}}^{\circ} + E_{\mathrm{O_2}}^{\mathrm{gas}}) \tag{9}$$

where $E_{M_x\mathrm{O}_y}^{\mathrm{bulk}}$ and E_M^{bulk} are the energies per formula unit of the relaxed bulk metal oxides $M_x\mathrm{O}_y = \mathrm{La_2O_3}$ and $\mathrm{ZrO_2}$ and metals M = La and Zr, respectively (obtained directly from DFT), and $\Delta H_{\mathrm{f},M_x\mathrm{O}_y}^{\circ}$ are the experimental standard enthalpies of formation of bulk $M_x\mathrm{O}_y$. The term $T^{\circ} S_{\mathrm{O_2}}^{\circ} = 0.634$ eV is obtained from experiment [48].

Only certain values of $\Delta\mu_{\mathrm{O}}$ are allowed [31]. The maximum value of $\Delta\mu_{\mathrm{O}}$, $(\Delta\mu_{\mathrm{O}})_{\mathrm{max}}$, is the value of $\Delta\mu_{\mathrm{O}}$ at 100 K and $p^{\circ}_{\mathrm{O}_2}$, the largest p_{O_2} that is relevant but below the p_{O_2} where a condensed phase of oxygen will form at 100 K. The minimum value of $\Delta\mu_{\mathrm{O}}$, $(\Delta\mu_{\mathrm{O}})_{\mathrm{min}}$, is the smallest value of $\Delta\mu_{\mathrm{O}}$ that can be achieved before one or more precipitates will form on the LZ surface. To determine $(\Delta\mu_{\mathrm{O}})_{\mathrm{min}}$, the conditions for which bulk LZ is thermodynamically preferred or in equilibrium with respect to bulk La, Zr, La_2O_3, and ZrO_2 are written as, respectively, Eqs. (10)−(13). These equations are then plotted.

$$\Delta\mu_{\mathrm{La}} \leq 0 \tag{10}$$

$$2\Delta\mu_{\mathrm{La}} + 7\Delta\mu_{\mathrm{O}} \geq \Delta E_{\mathrm{f,LZ}} \tag{11}$$

$$2\Delta\mu_{\mathrm{La}} + 3\Delta\mu_{\mathrm{O}} \leq \Delta E_{\mathrm{f,La_2O_3}} \tag{12}$$

$$2\Delta\mu_{\mathrm{La}} + 3\Delta\mu_{\mathrm{O}} \geq \Delta E_{\mathrm{f,LZ}} - 2\Delta E_{\mathrm{f,ZrO_2}} \tag{13}$$

where

$$\Delta E_{\mathrm{f,LZ}} = E^{\mathrm{bulk}}_{\mathrm{LZ}} - 2E^{\mathrm{bulk}}_{\mathrm{La}} - 2E^{\mathrm{bulk}}_{\mathrm{Zr}} - \frac{7}{2}E^{\mathrm{gas}}_{\mathrm{O_2}} \tag{14}$$

$$\Delta E_{\mathrm{f,La_2O_3}} = E^{\mathrm{bulk}}_{\mathrm{La_2O_3}} - 2E^{\mathrm{bulk}}_{\mathrm{La}} - \frac{3}{2}E^{\mathrm{gas}}_{\mathrm{O_2}} \tag{15}$$

$$\Delta E_{\mathrm{f,ZrO_2}} = E^{\mathrm{bulk}}_{\mathrm{ZrO_2}} - E^{\mathrm{bulk}}_{\mathrm{Zr}} - E^{\mathrm{gas}}_{\mathrm{O_2}} \tag{16}$$

Unlike $\Delta\mu_{\mathrm{O}}$, the value of $\Delta\mu_{\mathrm{La}}$ for a given set of conditions cannot be determined. However, once $\Delta\mu_{\mathrm{O}}$ is known, $\Delta\mu_{\mathrm{La}}$ is restricted to those values satisfying Eqs. (10)−(13).

A final constraint on the values of $\Delta\mu_{\mathrm{O}}$ and $\Delta\mu_{\mathrm{La}}$ is that the Ω must be positive. Otherwise, spontaneous formation of a surface and disintegration of the LZ crystal will occur.

2.5. Vibrational effects

The equations in the previous section are derived neglecting the effects of vibrational contributions. However, temperature-dependent vibrational contributions may be important, especially at high T, and need to be taken into account. Using equations and references in Ref. [31], Supporting Information, Section S6 as a starting point, the surface free energy of a LZ surface that includes approximate vibrational contributions can be written as

$$\tilde{\Omega}(T) = \Omega + \Omega^{\mathrm{vib}}(T) \tag{17}$$

where the vibrational contribution to $\tilde{\Omega}(T)$ is given by

$$\Omega^{\mathrm{vib}}(T) = \frac{3}{A}\sum_{a} \Gamma_{\mathrm{Zr},a} F^{\mathrm{vib,bulk}}_{\mathrm{LZ},a}(T) \tag{18}$$

and the terms $F^{\mathrm{vib,bulk}}_{\mathrm{LZ},a}(T)$ are obtained using

$$F^{\mathrm{vib,bulk}}_{\mathrm{LZ},a}(T) = \int F^{\mathrm{vib}}(T,\nu) g^{\mathrm{bulk}}_{\mathrm{LZ},a}(\nu) \mathrm{d}\nu \tag{19}$$

where

$$F^{\mathrm{vib}}(T,\nu) = \frac{1}{2}h\nu + k_{\mathrm{B}}T\ln(1 - e^{-h\nu/k_{\mathrm{B}}T}) \tag{20}$$

and $g^{\mathrm{bulk}}_{\mathrm{LZ},a}(\nu) = g^{\mathrm{bulk}}_{\mathrm{LZ,La}}(\nu)$ and $g^{\mathrm{bulk}}_{\mathrm{LZ,O}}(\nu)$ are, respectively, the normalized phonon DOS of bulk LZ's La atom and the normalized sum of six times the phonon DOS of bulk LZ's O atom plus the phonon DOS of bulk LZ's O′ atom, ν is the frequency, and h is Planck's constant. A procedure to show that Eq. (17) is accurate is discussed in the supplementary material, Section S.2.

In addition, $(\Delta\mu_{\mathrm{O}})_{\mathrm{max}}$, $(\Delta\mu_{\mathrm{O}})_{\mathrm{min}}$, and the allowed values of $\Delta\mu_{\mathrm{La}}$ at a given value of $\Delta\mu_{\mathrm{O}}$ need to be determined as a function of T. The determination of these quantities is discussed in the supplementary material, Section S.2.

3. Results and discussion

3.1. Energetic factors in determining surface stability

To achieve the objectives of this work as described at the end of Section 1, as a first step, the E_{su} and E_{sr} are computed. They are computed for every defective surface termination having an integer number of formula units using Eq. (1) and for every pair of complementary ideal surface terminations using Eq. (2). Results are given in Fig. 4. In addition, the E_{su} and E_{sr} can be computed for 10 pairs of defective (001) surface terminations using Eq. (2). Results for two of these pairs having the smallest and largest E_{sr} out of nine of the pairs and results for the remaining pair, the (001) n6 and n10 surfaces, are shown in Fig. 4. From Fig. 4, the trend of E_{su} results, shown by the striped open bars, is similar to that of E_{sr} results, shown by the filled bars. Thus, the relative stability of a surface termination or pair of surface terminations is determined, at least partially, by a purely energetic factor, namely, the number and strength of bonds broken per unit area in forming a surface termination. However, the correlation is not perfect, indicating that relative stability is also affected by surface restructuring. Examining Fig. 4 further, the defective (001) n2 surface is much more stable than both pairs of complementary ideal (001) surface terminations, with $E_{\mathrm{sr}} = 0.111$ eV/Å^2 versus 0.191 and 0.251 eV/Å^2, respectively, while the E_{sr} for all 10 pairs of defective (001) surface terminations are less than or equal to 0.174 eV/Å^2. Thus, a defective (001) surface may be preferred over a large set of T and $p_{\mathrm{O_2}}$ conditions. In addition, E_{sr} for the defective (111) n2 and n3, n1 and n4, and n1 and n5 surfaces can be computed and are 0.071, 0.122, and 0.125 eV/Å^2, respectively. Note that E_{su} for these pairs of defective (111) surface terminations are not given, because the adsorbed oxygen atoms are not in positions that can be occupied in the bulk crystal. The E_{sr} of the (111) n2 and n3 surfaces, 0.071 eV/Å^2, is smaller than the E_{sr} of the different pairs of complementary ideal (111) surface terminations. Thus, a defective (111) surface may also be preferred over a set of T and $p_{\mathrm{O_2}}$ conditions. Although defective (001) and (111) surfaces may be preferred, the stabilities of individual ideal surface terminations are not given in Fig. 4, making it impossible to compare directly the stabilities of individual ideal and defective surface terminations. Also, the effect of the environment on stabilities is not taken into account. For these reasons, a different metric is needed to determine the preferred surface terminations of a surface, that is, the Ω, which is

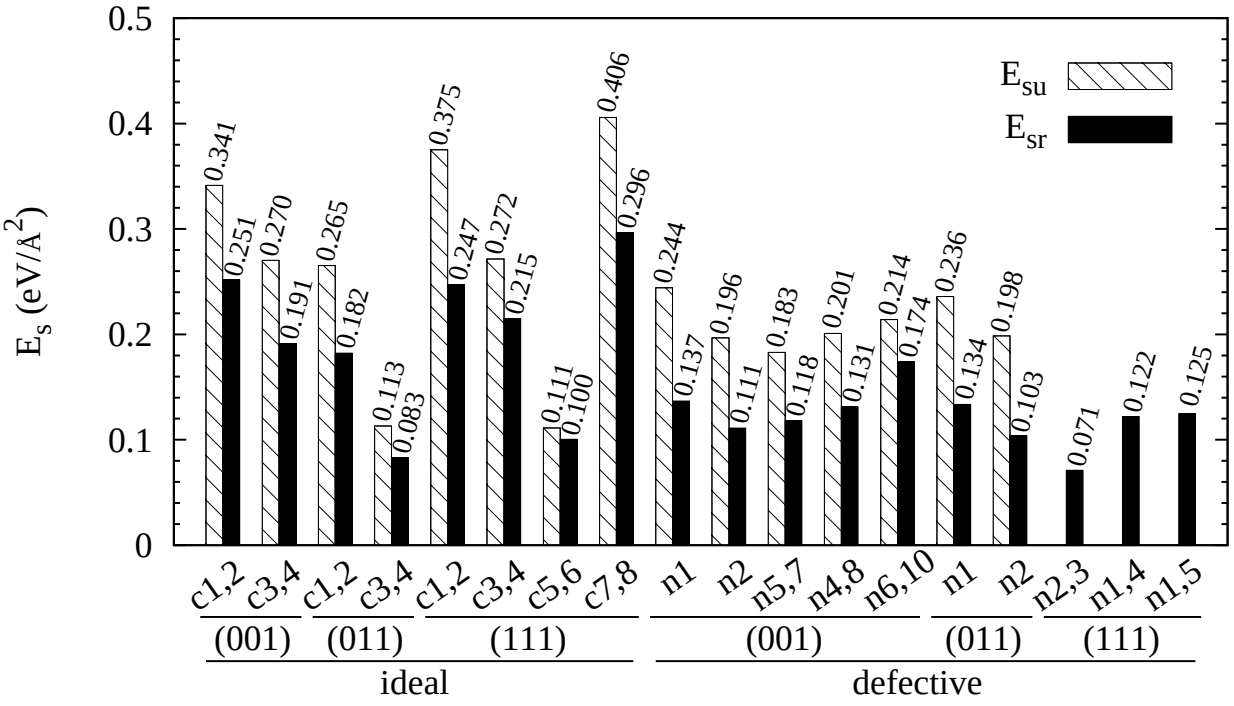

Figure 4: The $E_{\rm su}$ and $E_{\rm sr}$ of pairs of complementary ideal, certain defective, and certain pairs of defective surface terminations. Pairs of surface terminations are designated using a shorthand in the figure. For example, the (001) c1 and c2 surfaces are designated (001) c1,2.

examined in the next section.

3.2. Preferred surface terminations as a function of T and p_{O_2}

To achieve the goal of this section, a few steps need to be taken. First, the Ω and the allowed values of the variables $\Delta\mu_{\rm O}$ and $\Delta\mu_{\rm La}$ in the expression for Ω need to be determined. The Ω of a LZ surface termination is given by Eq. (3) and expressed in terms of the constants $\phi_{\rm Zr}$, $\Gamma_{{\rm Zr},a}$, and A. These constants for the different surface terminations are given in Table 1. Next, $(\Delta\mu_{\rm O})_{\rm max} = 0.26$ eV using Eq. (8), $\delta\mu^{\circ}_{\rm O} = 0.06$ eV. Lastly, Eqs. (10)$-$(13) are plotted using computed values of $\Delta E_{\rm f,LZ}$, $\Delta E_{\rm f,La_2O_3}$, and $\Delta E_{\rm f,ZrO_2}$ to determine $(\Delta\mu_{\rm O})_{\rm min} = -5.44$ eV and the allowed values of $\Delta\mu_{\rm La}$ at every value of $\Delta\mu_{\rm O}$.

Having determined the Ω and allowed values of $\Delta\mu_{\rm O}$ and $\Delta\mu_{\rm La}$, the preferred surface termination of the different surfaces can be identified as a function of $\Delta\mu_{\rm O}$. From Table 1, $\Gamma_{\rm Zr,La} = 0$ for the (001) and (011) surface terminations. Thus, the Ω of the (001) and (011) surface terminations are linear functions of $\Delta\mu_{\rm O}$. The Ω of the (001) surface terminations are plotted as a function of $\Delta\mu_{\rm O}$ in Fig. 5, top panel. As $\Delta\mu_{\rm O}$ is decreased from $(\Delta\mu_{\rm O})_{\rm max}$ down to $(\Delta\mu_{\rm O})_{\rm min}$, the (001) surface termination with the smallest value of Ω is predicted to change

Table 1: The $\Gamma_{\mathrm{Zr},a}$ [Eq. (7)] and ϕ_{Zr} (eV) [Eq. (6)] of the different surface terminations[a]

termination	$\Gamma_{\mathrm{Zr,La}}$	$\Gamma_{\mathrm{Zr,O}}$	ϕ_{Zr}
(001) c1	0	3.5	5.38
c2	0	−3.5	24.44
c3	0	2.5	4.07
c4	0	−2.5	18.55
n1	0	0	8.12
n2	0	0	6.59
n3	0	0.5	6.08
n4[b]	0	0.5	6.31
n5	0	0.5	5.88
n6	0	1.5	6.98
n7[b]	0	−0.5	8.10
n8	0	−0.5	9.22
n9	0	−0.5	8.49
n10	0	−1.5	13.68
(011) c1	0	3.5	5.87
c2	0	−3.5	24.71
c3	0	0.5	5.96
c4	0	−0.5	7.97
n1[b]	0	0	11.22
n2	0	0	8.66
n3	0	0.5	7.12
n4	0	0.5	5.50
n5	0	1.5	7.26
n6	0	1.5	7.97
n7	0	1.5	6.66
n8	0	3.5	6.92
n9	0	1.5	5.35
n10	0	2.5	5.34
n11	0	2.5	4.94
n12	0	4.5	4.94
(111) c1[c]	−1	1.75	11.50
c2	1	−1.75	13.88
c3	−1	0.75	15.06
c4	1	−0.75	7.00
c5	1	2.25	−5.92
c6	−1	−2.25	16.22
c7	1	5.25	−3.44
c8	−1	−5.25	33.86
n1	1	0.25	0.83
n2	1	1.25	−4.83
n3	−1	−1.25	12.14
n4	−1	−0.25	11.97
n5	−1	−0.25	11.68
n6	−1	−4.25	27.62
n7	−1	−3.25	21.53

[a]For (001), (011), and (111) surface terminations, A = 59.296, 83.857, and 51.352 Å^2, respectively. [b,c]The relaxed structure is obtained from a starting structure that is obtained from a relaxed structure [b]using the CA functional or [c]at a higher PW91 level of theory, as described in the supplementary material, Section S.1.

from c3 to n5 to n2 to n7 to c4. Thus, only five (001) surface terminations are preferred out of the large set of (001) surface terminations considered. The relaxed structures of these preferred surface terminations are shown in an appendix, Fig. A.1. The identification of preferred (001) surface terminations made here is physically reasonable. A decrease in $\Delta\mu_{\mathrm{O}}$ is equivalent to a change from low T, high p_{O_2}, or both of these conditions in the reservoir system with which the (001) surface is in equilibrium to high T, low p_{O_2}, or both of these conditions. Thus, as $\Delta\mu_{\mathrm{O}}$ is lowered, the preferred (001) surface termination is expected to change from oxygen-rich, with a large positive value of $\Gamma_{\mathrm{Zr,O}}$, to oxygen-poor, with a large negative value of $\Gamma_{\mathrm{Zr,O}}$. This trend is exactly observed in Fig. A.1. In addition, another trend is predicted. The Ω of a (001) surface termination is predicted to increase with respect to other (001) surface terminations of the same type, either ideal or defective, with increasing polarity of the unrelaxed surface termination assuming formal ionic charges for atoms. This trend is predicted despite the use of symmetric slab models, because Ω is also correlated with E_{su} and, thus, the number and strength of bonds broken in forming the surface. The E_{su} of an ideal surface termination is not possible to compute directly. However, it is estimated as one half of E_{su} of the ideal surface termination and its complement shown in Fig. 4. This estimate is expected to be reasonably accurate, because the same types and numbers of bonds are broken in forming complementary ideal surface terminations of the (001), (011), or (111) surfaces. Comparing ideal surface terminations in Fig. 5, top panel, the (001) c3 and c4 surfaces are more stable than the (001) c1 and c2 surfaces over a range of $\Delta\mu_{\mathrm{O}}$ values. The unrelaxed (001) c3 and c4 surfaces are less polar than the unrelaxed (001) c1 and c2 surfaces, with alternating layer and multilayer unit charges of $\pm 10e$ versus $\pm 14e$, respectively, as shown in Fig. 2, and have a smaller E_{su}. Comparing defective (001) surface terminations in Fig. 5, top panel, the (001) n5, n2, and n7 surfaces are quite stable, while the (001) n3, n4, n8, and n9 surfaces are slightly less stable, and the (001) n6 and n10 surfaces are much less stable over a range of $\Delta\mu_{\mathrm{O}}$ values. As discussed in Ref. [31], a LZ surface termination is nonpolar if the sum of formal ionic charges in the topmost layer or multilayer is half that of a bulk Lp unit. The unrelaxed (001) n2 surface is a (001) c2 surface with one La and one Zr atom vacancy per surface unit cell and, thus, is nonpolar. It is also described by a small E_{su}. The (001) n3−n5 and n7−n9 surfaces are (001) c3 surfaces with two and three oxygen

atoms removed per surface unit cell, respectively, and are nearly polarity compensated, with formal charges in the topmost atomic layer of $-6e$ and $-4e$, respectively, compared to a value of $-5e$ required for surface polarity compensation. Different pairs of these surfaces are described by small $E_{\rm su}$. The unrelaxed (001) n6 and n10 surfaces are (001) c3 surfaces with one and four oxygen vacancies per surface unit cell, respectively, are not as close to being polarity compensated, and have a larger $E_{\rm su}$.

A similar analysis can be done for the (011) surface. From Fig. 5, middle panel, the preferred (011) surface termination is predicted to change from n12 to n11 to n4 to c4. Relaxed structures of these surface terminations are shown in an appendix, Fig. A.2. Again, only a few (011) surface terminations are preferred, and the preferred surface termination is observed to change from oxygen-rich to -poor. Also, an increase of Ω with surface polarity is predicted. For example, as shown in Fig. 5, middle panel, the (011) c3 and c4 surfaces are much more stable than the (011) c1 and c2 surfaces over a range of $\Delta\mu_{\rm O}$ values. The unrelaxed (011) c3 and c4 surfaces are much less polar than the unrelaxed (011) c1 and c2 surfaces, with alternating unit charges of $\pm 2e$ versus $\pm 14e$, respectively, as shown in Fig. 2, and have a much smaller $E_{\rm su}$.

The preferred (111) surface terminations are also straightforwardly determined. From Table 1, $\Gamma_{\rm Zr,La} \neq 0$ for the (111) surface terminations. Thus, the Ω of the (111) surface terminations are linear functions of two variables, $\Delta\mu_{\rm O}$ and $\Delta\mu_{\rm La}$. The (111) surface termination with the smallest value of Ω as a function of $\Delta\mu_{\rm O}$ and $\Delta\mu_{\rm La}$ is shown in Fig. 5, bottom panel. In this figure, the labeled regions are where (111) surface terminations are identified as preferred. For example, in the region labeled "c1", the preferred (111) surface termination is c1. Outside of these regions, one or more Ω are negative, and no surface termination is identified as preferred. The solid black lines labeled "La/Zr/La_2O_3/ZrO_2 precipitation line" are Eqs. (10)−(13), respectively. The region that is formed by three of these lines and the dot−dashed black line corresponding to $(\Delta\mu_{\rm O})_{\rm max}$ is shown in color, or as segments of different color. This region is the only part of the figure where, for allowed values of $\Delta\mu_{\rm O}$, one or more precipitates will not form on the LZ surface. The value of $(\Delta\mu_{\rm O})_{\rm min}$ is given by the location of this region's upper left corner at $\Delta\mu_{\rm O} = -5.44$ eV, while the allowed values of $\Delta\mu_{\rm La}$ at a given value of $\Delta\mu_{\rm O}$ are shown graphically. The different color segments are

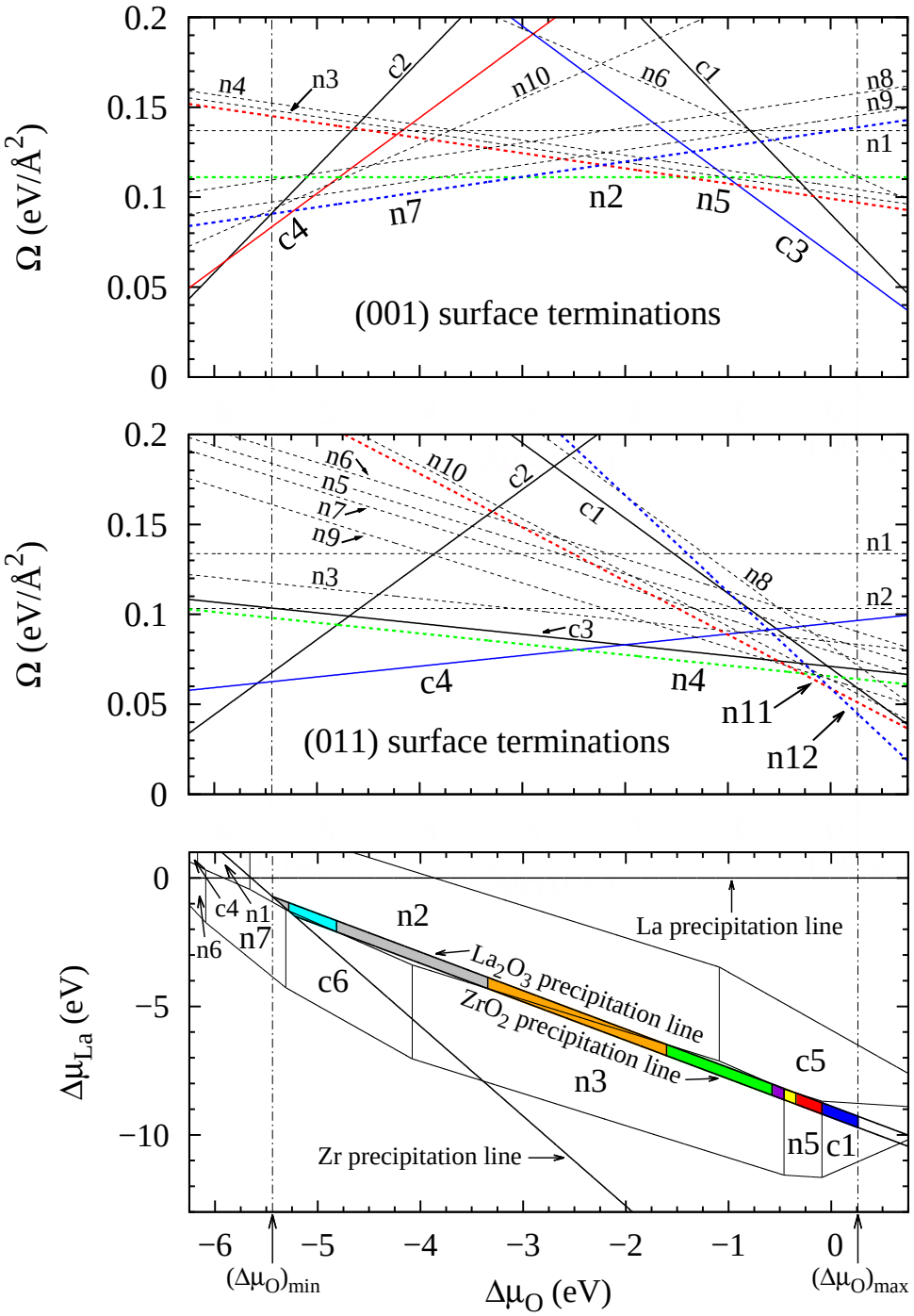

Figure 5: (Top and middle) The Ω of the (top) (001) and (middle) (011) surface terminations as a function of $\Delta\mu_O$. The Ω of the ideal and defective surface terminations of a given surface are plotted using solid and dashed lines, respectively. The Ω of preferred surface terminations are plotted in color. (Bottom) The (111) surface termination with the smallest value of Ω as a function of $\Delta\mu_O$ and $\Delta\mu_{La}$. See the text for further discussion. (For interpretation of the reference to color in this figure legend, the reader is referred to the web version of this article.)

where different (111) surface terminations are preferred. For example, only one (111) surface termination, c1, is contained in and on the borders of the blue region. Thus, the preferred (111) surface termination is c1 for values of $\Delta\mu_O$ given by the blue region. However, two (111) surface terminations, n3 and n2, are contained in and on the borders of the orange region. Thus, the preferred (111) surface termination is either n3 or n2 for values of $\Delta\mu_O$ given by the orange region. As $\Delta\mu_O$ is decreased, the preferred (111) surface termination is predicted to change from c1 for values of $\Delta\mu_O$ given by the blue region, to n5 for values of $\Delta\mu_O$ given by the red region, to n5 or c5 for values of $\Delta\mu_O$ given by the yellow region, to c5 or n3 to n3 to n3 or n2 to n2 to n2 or c6 to n2. Relaxed structures of these surface terminations are shown in an appendix, Fig. A.3.

By converting the values of $\Delta\mu_O$ for which a surface termination is preferred into conditions of T and p_{O_2}, the preferred surface termination of a surface can be identified as a function of external conditions. This conversion is done using Eq. (8). To illustrate how it is done, Eq. (8) is plotted to show the relation between a value of $\Delta\mu_O$ and different T and p_{O_2} pairs in Fig. 6. The preferred surface termination of the (001), (011), and (111) surfaces is shown as a function of T and log (p_{O_2} / 1 atm) in SPDs, Fig. 7, left column. In the SPDs, the regions in color are where surface terminations are identified as preferred. For example, in Fig. 7, left column, bottom panel, in the blue region labeled "c1", the preferred (111) surface termination is c1. The white area in the different SPDs labeled "Precipitate(s) form" is where one or more precipitates will form on the LZ surface and is obtained by converting $(\Delta\mu_O)_{\min}$ into conditions of T and p_{O_2}. In addition, a region is shown labeled "Breakdown of SHA", where SHA is defined as Standard Harmonic Approximation. In this region, results can only be estimated, as discussed in the next section. Lastly, because log (p_{O_2} / 1 atm) is plotted, the range of p_{O_2} values represented in these SPDs is from 1 to 10^{-100} atm. In principle, extremely low values of p_{O_2} can be achieved if a reducing agent is present [49], providing a basis for the range's lower limit. The conclusion from the SPDs is that, for the different surfaces, defective surface terminations are preferred over large sets of T and p_{O_2} values.

In addition to the above results needed to obtain the SPDs, other results are also of interest. Upper and lower limits on the Ω of the (111) surface terminations as a function of

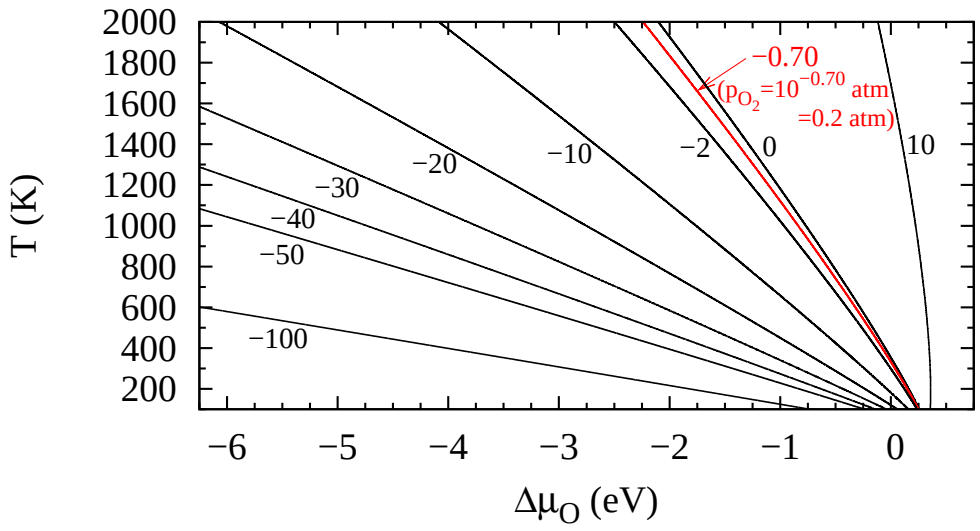

Figure 6: Relation between $\Delta\mu_O$ and different T and p_{O_2} pairs using Eq. (8), $\delta\mu_O^\circ = 0.06$ eV. The values of p_{O_2} are given by the isobar lines. The p_{O_2} in atm represented by a line is equal to 10 raised to the power of the number m next to the line: $p_{O_2} = 10^m$ atm.

$\Delta\mu_O$ and a phase diagram identifying the precipitate or precipitates that will form on the LZ surface as a function of $\Delta\mu_O$ and $\Delta\mu_{La}$ are given in the supplementary material, Section S.3. Also, a trend of increasing Ω with surface polarity is predicted for several other surface terminations. This trend is discussed in the supplementary material, Section S.3. On a different note, to identify the preferred surface termination out of all surface terminations considered, an analysis similar to that given for the (111) surface terminations is performed for (001), (011), and (111) surface terminations in the supplementary material, Section S.3.

3.3. Validation of results

In this section, a comparison is made to the only other theoretical study [50] of a pyrochlore oxide's surfaces besides Refs. [29–31] before examining how the SPDs obtained in the previous section are affected by vibrational effects and level of theory. In Ref. [50], the stabilities of different $Y_2Ti_2O_7$ (001) and (011) surface terminations are determined by computing surface free energies. Using the surface nomenclature in this work, the preferred $Y_2Ti_2O_7$ (001) surface termination is predicted to change from c3 to n1 or n2 to c2 with decreasing $\Delta\mu_O$, with n1 being only slightly more stable than n2, while c1 is unstable. The preferred $Y_2Ti_2O_7$ (011) surface termination is predicted to change from c1 to c3 to c4 to c2 with decreasing $\Delta\mu_O$, with n1 being unstable but slightly more stable than n2, which, in

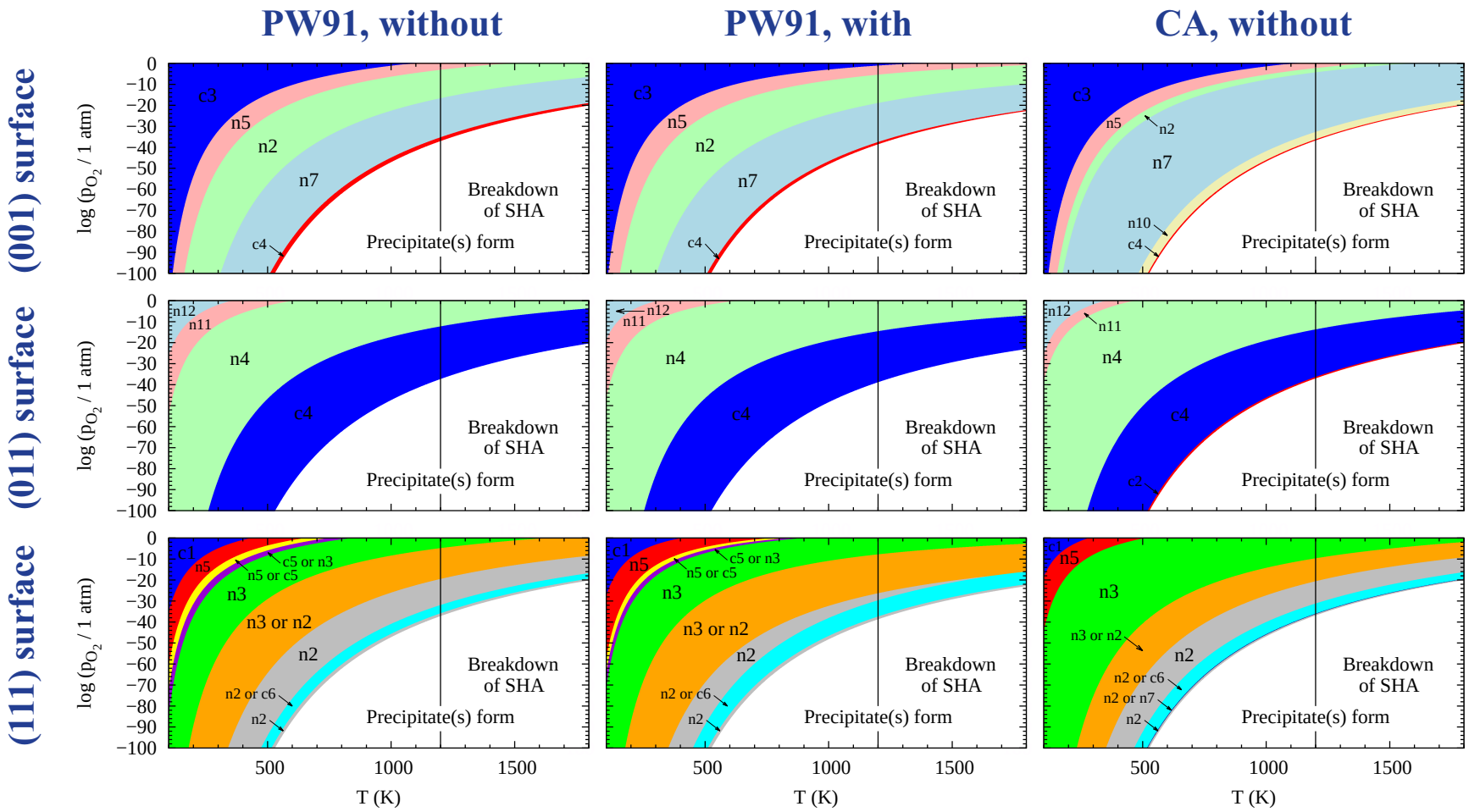

Figure 7: The SPDs of the (top row) (001), (middle row) (011), and (bottom row) (111) surfaces (left column) without and (middle column) with vibrational contributions and (right column) at the CA level of theory. The colors of regions are chosen to be consistent with those used to indicate preferred surface terminations in Fig. 5 and in figures provided in the supplementary material, i.e., Figs. S.13−S.15 and S.21. Thus, the relation between a set of $\Delta\mu_O$ values and conditions of T and p_{O_2} is emphasized. Also, regions are shown where one or more precipitates will form on the surface, labeled "Precipitate(s) form", and a region is shown where results can only be estimated, labeled "Breakdown of SHA". (For interpretation of the reference to color in this figure legend, the reader is referred to the web version of this article.)

turn, is more stable than two other defective (011) surface terminations. These results are consistent with those given in this work, except that the stabilities of the (001) n1 and n2 surfaces and (011) n1 and n2 surfaces are inverted. Importantly, the two least stable defective $Y_2Ti_2O_7$ (011) surface terminations are relatively unstable, providing additional support for neglecting the equivalent LZ (011) surface terminations. These surface terminations are formed by removing atoms from a L8-terminated surface and are not examined here or in Ref. [31] because a stable surface unit formed upon relaxation of this surface would have to be broken [31].

3.3.1. Vibrational effects

To verify the SPDs obtained in Section 3.2, they need to be redetermined by taking into account vibrational contributions. The $\Omega^{\text{vib}}(T)$ for the different surface terminations are computed using Eq. (18). In this equation, the $F_{\text{LZ},a}^{\text{vib,bulk}}(T)$ are computed using $g_{\text{LZ},a}^{\text{bulk}}(\nu)$. Because reference $g_{\text{LZ},a}^{\text{bulk}}(\nu)$ are not available, $g_{\text{LZ},a}^{\text{bulk}}(\nu)$ are computed as part of this work. The $F_{\text{LZ},a}^{\text{vib,bulk}}(T)$ that are obtained are expected to be accurate. The reason is that vibrational contributions to free energies are relatively insensitive to error in phonon DOSs [51]. This fact is illustrated in the supplementary material, where vibrational contributions from different atom types to the free energies of bulk M and M_xO_y are obtained from computed phonon DOSs and compared to results obtained using phonon DOSs from the literature, or reference phonon DOSs. Despite some significant differences in the computed and reference phonon DOSs of bulk ZrO_2, the computed and reference vibrational contributions are similar. The $\Omega^{\text{vib}}(T)$ of selected surface terminations are shown in Fig. 8. In addition to the results mentioned above, several other results pertaining to the determination of $\Omega^{\text{vib}}(T)$ are given in the supplementary material, Section S.4, including: the $\Omega^{\text{vib}}(T)$ of all surface terminations, the computed and reference phonon DOSs of bulk M and M_xO_y, a comparison of the computed and reference [52] phonon DOSs of bulk ZrO_2 to phonon DOSs from Refs. [53–55], the first computation of the phonon DOSs of the two different atom types in bulk La, thereby building on previous work [56], computed phonon DOSs and vibrational contributions to the free energy of bulk LZ, a demonstration that the $\Omega^{\text{vib}}(T)$ are good approximations to $\Omega^{\text{vib,exact}}(T)$, and a comparison of $\Omega^{\text{vib}}(T)$ to the exact vibrational contribution to the surface

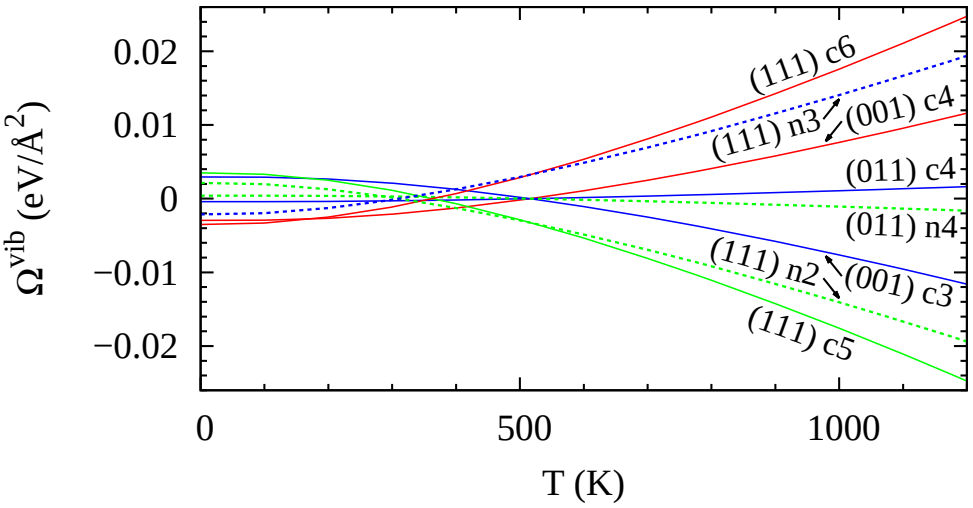

Figure 8: The $\Omega^{\text{vib}}(T)$ of selected (001), (011), and (111) surface terminations as a function of T.

free energy of the (001) c3 surface obtained from a computed phonon DOS.

Using the $\Omega^{\text{vib}}(T)$ as well as new values of $(\Delta\mu_{\text{O}})_{\text{max}}$, $(\Delta\mu_{\text{O}})_{\text{min}}$, and new allowed values of $\Delta\mu_{\text{La}}$, new SPDs are obtained, Fig. 7, middle column. The original SPDs shown in Fig. 7, left column are similar to these new SPDs, with the largest changes in the SPD of the (111) surface. Thus, the original SPDs can be used for further analysis. Note that the new SPDs are only accurate at or below 1200 K. The reason is that the SHA made to evaluate the terms $F_{\text{LZ},a}^{\text{vib,bulk}}(T)$ is expected to breakdown above roughly half of the melting point of bulk LZ [52]. The melting point of bulk LZ is 2433−2613 K [57]. By contrast, the vibrational contributions to the free energies of bulk M and M_xO_y that are used to determine $(\Delta\mu_{\text{O}})_{\text{min}}$ and the allowed values of $\Delta\mu_{\text{La}}$ at a given value of $\Delta\mu_{\text{O}}$ as a function of T are still expected to be accurate at $T \approx 1200-1300$ K, for reasons similar to those given in Ref. [31], Supporting Information, Section S6. Thus, the new SPDs are limited by the accuracy of the $F_{\text{LZ},a}^{\text{vib,bulk}}(T)$ terms and are concluded to be accurate at or below 1200 K. As a result, the original SPDs can only be verified up to 1200 K. As a reminder of these facts, the regions above 1200 K in both sets of SPDs are labeled "Breakdown of SHA".

In addition to the above results, the $\tilde{\Omega}(T)$ of the (001) and (011) surface terminations as a function of $\Delta\mu_{\text{O}}$, the (111) surface termination with the smallest $\tilde{\Omega}(T)$ as a function of $\Delta\mu_{\text{O}}$ and $\Delta\mu_{\text{La}}$, and upper and lower limits on the $\tilde{\Omega}(T)$ of the (111) surface terminations

as a function of $\Delta\mu_{\mathrm{O}}$ at selected T are provided in the supplementary material, Section S.4. Also, two-dimensional maps giving the preferred surface termination out of all surface terminations considered as a function of $\Delta\mu_{\mathrm{O}}$ and $\Delta\mu_{\mathrm{La}}$ and taking into account vibrational contributions are given at selected T, and a SPD depicting the preferred surface termination out of all surface terminations considered as a function of T and log (p_{O_2} / 1 atm) and taking into account vibrational contributions is given in the supplementary material, Section S.4.

3.3.2. Level of theory

Also to verify the original set of SPDs, the level of theory used to obtain these SPDs needs to be justified. As done in Ref. [31], SPDs obtained within the LDA using the CA functional are obtained, Fig. 7, right column. These diagrams are readily obtained from the results of this work. They are similar to those shown in Fig. 7, left column, with the biggest differences in the SPDs of the (001) and (111) surfaces. Weakly correlated oxides such as LZ can be described well at either level of theory. Thus, the fact that the two sets of SPDs are similar is evidence that both sets of SPDs are accurate. As done in obtaining the original set of SPDs, plots of Ω of the (001) and (011) surface terminations, a plot of the preferred (111) surface termination as a function of $\Delta\mu_{\mathrm{O}}$ and $\Delta\mu_{\mathrm{La}}$, a plot showing the relation between a value of $\Delta\mu_{\mathrm{O}}$ and different T and p_{O_2} pairs, and plots of the limits of Ω of the (111) surface terminations using the CA functional are also provided. These results are provided in the supplementary material, Section S.5.

Next, errors in the original SPDs due to the choice of PW91 method are addressed. One source of error are the terms $\Delta E_{\mathrm{f},M_x\mathrm{O}_y}$ and $\Delta E_{\mathrm{f,LZ}}$. For the (111) surface, the region where bulk LZ is thermodynamically preferred will be shifted by error in these terms, affecting the identification of preferred (111) surface terminations [58]. However, computed values of these terms are reasonably accurate compared to experimental values. The computed values of $\Delta E_{\mathrm{f},\mathrm{La_2O_3}}$, $\Delta E_{\mathrm{f},\mathrm{ZrO_2}}$, and $\Delta E_{\mathrm{f,LZ}}$ are -17.77, -10.45, and -39.54 eV/formula unit, respectively. The corresponding experimental enthalpies of formation at standard conditions, $\Delta H^{\circ}_{\mathrm{f},\mathrm{La_2O_3}}$, $\Delta H^{\circ}_{\mathrm{f},\mathrm{ZrO_2}}$, and $\Delta H^{\circ}_{\mathrm{f,LZ}}$, are -18.59 [48], -11.41 [48], and -42.52 eV/formula unit [59], respectively. The computed terms are reasonably accurate, because bulk $M_x\mathrm{O}_y$ and LZ are weakly correlated oxides with formally empty d and f shells. Thus, the error in $\Delta E_{\mathrm{f},M_x\mathrm{O}_y}$

and $\Delta E_{\mathrm{f,LZ}}$ is due mostly to error in $E_{\mathrm{O_2}}^{\mathrm{gas}}$ [60, 61]. Even if the errors in $\Delta E_{\mathrm{f},M_x\mathrm{O}_y}$ and $\Delta E_{\mathrm{f,LZ}}$ were larger, for a large fraction of $\Delta\mu_{\mathrm{O}}$ values, the preferred (111) surface termination is defective at all values of $\Delta\mu_{\mathrm{La}}$ for which the Ω are positive, as shown in Fig. 5, bottom panel. Thus, a defective (111) surface would still be predicted over a large set of T and $p_{\mathrm{O_2}}$ conditions. Similarly, although the value of $(\Delta\mu_{\mathrm{O}})_{\mathrm{min}}$ is affected by error in $\Delta E_{\mathrm{f},M_x\mathrm{O}_y}$ and $\Delta E_{\mathrm{f,LZ}}$, conditions of bulk LZ decomposition are not. The reason is that the error in $E_{\mathrm{O_2}}^{\mathrm{gas}}$ is subtracted out in converting $(\Delta\mu_{\mathrm{O}})_{\mathrm{min}}$ into conditions of T and $p_{\mathrm{O_2}}$. In fact, conditions of bulk LZ decomposition are very similar at PW91 and CA levels of theory, as shown in Fig. 7, left and right columns. Lastly, to test the convergence of results, the constants ϕ_{Zr} in Table 1 are recomputed for several of the surface terminations at a higher PW91 level of theory using a 600-eV cutoff and increasing the precision of the fast Fourier transform grids in the computations by specifying the VASP keyword PREC = Accurate. The original ϕ_{Zr} are very similar to the new ϕ_{Zr}, with average and maximum absolute differences of only 0.03 and 0.08 eV, respectively, indicating that they are well converged.

Having shown that the theory-dependent errors described above are small or can be neglected, the GGA and LDA methods used in this work are expected to be accurate. A remaining issue is that several of the defective surface terminations examined in this work are, in effect, ideal surface terminations with one or more oxygen atoms removed. Thus, like an oxygen vacancy in a bulk oxide forming a color center, one or more sites at these surface terminations may exist that tend to localize electronic charge. This effect may be significant and not captured by the GGA and LDA methods used here, in which case, the Ω of these surface terminations may be significantly underestimated. However, most of the defective surface terminations that can be described as having surface oxygen vacancies are characterized by a high density of these sites, including nearly all of the preferred defective surface terminations with these sites. For example, the preferred (001) n5 and n7 surfaces can be described as having two and three oxygen vacancies per surface unit cell, respectively. These sites are not expected to localize electrons due to repulsion of nearby electrons. Moreover, a trend is observed between the Ω and polarity of a surface's defective surface terminations that is physically reasonable, as discussed in Section 3.2 and the supplementary material, suggesting that the stabilities of defective surface terminations are accurately

predicted. Thus, GGA and LDA methods are used to predict the stabilities of different LZ surface terminations, as in several other theoretical studies of polar oxide surfaces modified by introducing oxygen vacancies [50, 62–65].

3.4. Implications of results and comparison to experiment

The main results of this work are the SPDs shown in Fig. 7, left column. Importantly, the preferred surface termination of a surface at a given set of T and p_{O_2} conditions cannot be conclusively identified from these SPDs. The reason is that only certain surface terminations of a surface are considered in this work, not every possible surface termination of the surface. Despite this limitation, important conclusions can still be drawn. First, only a few surface terminations of a surface are preferred out of those considered. More importantly, the preferred surface termination of a surface is shown to be defective instead of ideal over a large range of T and p_{O_2} conditions. Because every possible ideal surface termination of a surface is considered in this work, the preferred surface termination is able to be characterized as nonideal over the entire range of T and p_{O_2} conditions where defective surface terminations are preferred. The composition and structure of a surface may also depend on kinetic effects not considered in this work. However, the finding that the preferred surface termination of a surface is nonideal over a large range of T and p_{O_2} conditions is significant evidence for a nonideal surface termination of the surface over that range of conditions. The SPDs are the first evidence that the (011) and (111) surfaces are nonideal under large sets of T and p_{O_2} conditions and that the (001) surface is nonideal under a slightly larger set of conditions than previously reported [31], as seen by comparing the conditions for which a defective (001) surface termination is preferred in Fig. 7, top row, left column to those in Ref. [31], Supporting Information, Fig. S9, top row, middle column. To summarize these findings, new SPDs are made by relabeling the regions in Fig. 7, left column where an ideal surface termination is definitely not preferred as "Nonideal", relabeling all other regions with a "?" to indicate a preferred surface termination that is either ideal or nonideal, and combining like regions. The resultant SPDs are shown in Fig. 9.

In addition to these conclusions, a comparison to experiment is proposed in which certain Wulff shapes are made for comparison to experimental crystal shapes. Because every possible

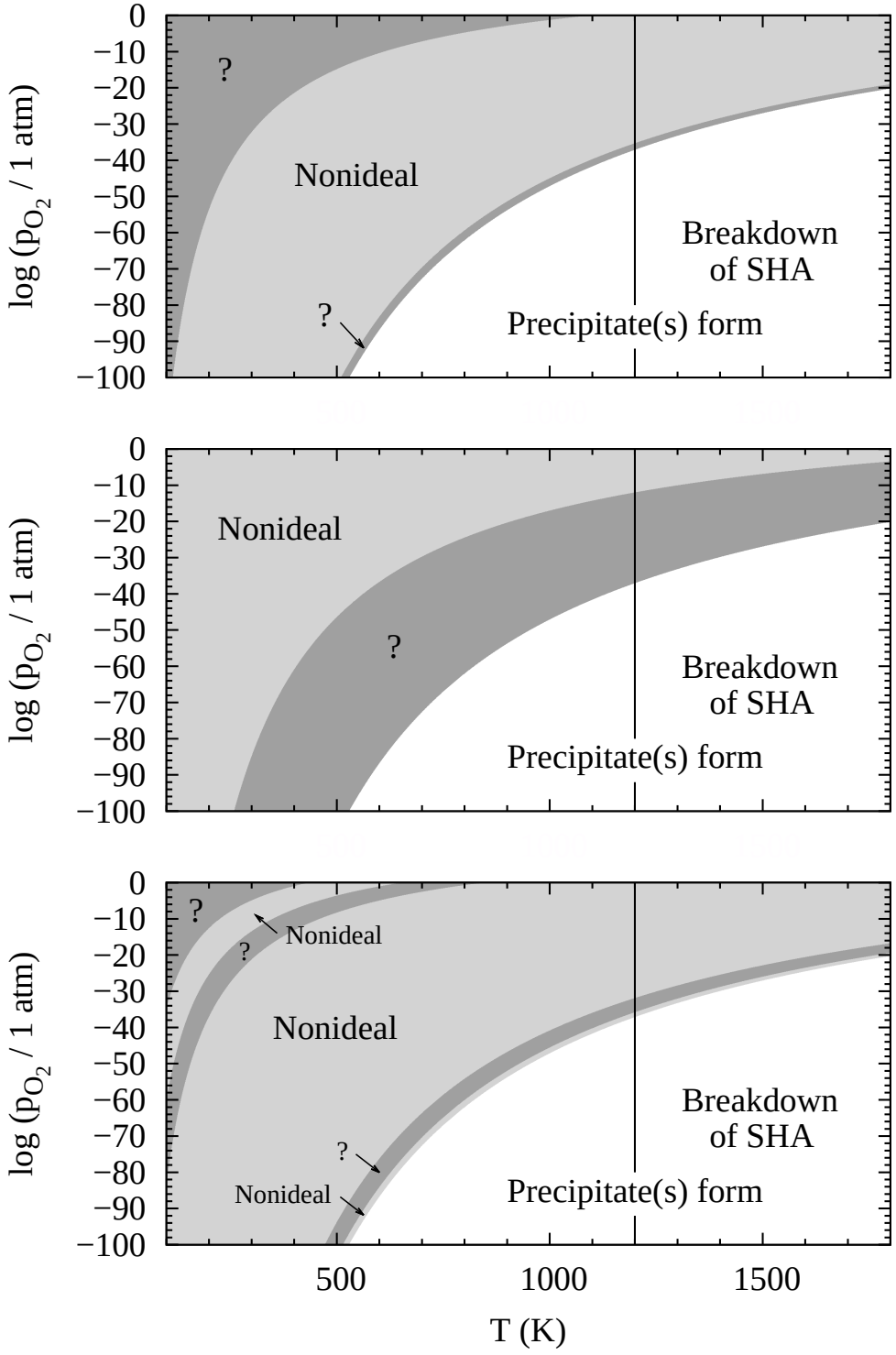

Figure 9: The SPDs in Fig. 7, left column redrawn to provide structural descriptions of the (top) (001), (middle) (011), and (bottom) (111) surfaces as a function of T and log (p_{O_2} / 1 atm). The labels "Nonideal" and "?" are defined in the text.

ideal surface termination of a surface is considered in this work, Wulff shapes are made based on preferred ideal surface terminations at different T and p_{O_2} conditions. These Wulff shapes can then be compared to experimental crystal shapes to show that the shapes are different and, thus, at least one surface of the experimental shape may be nonideal. This comparison is not made in this work, because the experimental shapes still need to be obtained to permit the comparison. The detailed comparison that is proposed is as follows. Wulff shapes are made using Ω of the most stable ideal (001), (011), and (111) surface terminations at values of $\Delta\mu_O$ corresponding to ambient conditions of 0.2 atm O_2 gas and 298.15 K and LZ synthesis conditions of 0.2 atm O_2 gas and 513 [25], 1173 [22–24], and 1473 K [26]. Note that, at a given set of conditions, Ω of the most stable ideal (111) surface termination is dependent on $\Delta\mu_{La}$ and will span a range of values. Thus, at every set of conditions, two Wulff shapes are made using the smallest and largest Ω of the most stable ideal (111) surface termination, to show the range of predicted Wulff shapes at those conditions. Results are shown in Fig. 10. A comparison can then be made to experimental crystal shapes. If the experimental shape at a given set of conditions is different from the two Wulff shapes shown at those conditions or any shape in between these shapes, then one or more surfaces of the experimental shape may be nonideal. For example, in an experimental study of LZ crystallites prepared at 0.2 atm O_2 gas and 1173 K, the crystallites are described as square-like [22]. If square-like is assumed to mean cubic, then the (001) surface is represented in the experimental crystal shape but not in the two Wulff shapes shown at 0.2 atm O_2 gas and 1173 K or any shape in between these shapes. To be represented in the predicted Wulff shapes, the (001) surface would need to have a value of Ω that is lower than that of the most stable ideal (001) surface termination. Thus, the (001) surface of the experimental shape must be nonideal, at least from a thermodynamic point of view. However, before a comparison such as this one can be made, more experimental work needs to be done. First, the distributions of shapes in synthesized LZ samples need to be accurately determined, and the shapes shown to have the (001), (011), and (111) surfaces. This work can be done following Ref. [66]. In addition, the extent to which particle shape and size is controlled by kinetic effects as well as external factors such as solvent effects needs to be studied, as done to a limited extent in Ref. [23]. The predicted Wulff shapes are made using the Gibbs−Wulff theorem stating that

the distance of a surface from the center of the crystal shape is proportional to Ω. Thus, a ratio of crystallite thicknesses perpendicular to the (001) and (011) surfaces or range of ratio values of crystallite thicknesses perpendicular to the (001) or (011) and (111) surfaces can also be compared to an experimental value. Examples of ratios of the crystallite thickness perpendicular to the (001) surface divided by the crystallite thickness perpendicular to the (011) surface are provided in Ref. [31], Supporting Information, Section S8. Note that the error in a predicted Wulff shape or ratio value due to the choice of method or neglect of vibrational contributions is minor, based on results obtained using the CA functional or taking into account vibrational contributions. Lastly, Wulff shapes obtained using Ω of preferred surface terminations, versus preferred ideal surface terminations, are provided to allow a direct comparison to experimental crystal shapes. They are provided despite the fact that the preferred surface termination of a surface cannot be conclusively identified, as stated at the beginning of Section 3.4, and, therefore, the predicted and experimental shapes may be different. The Wulff shapes based on preferred surface terminations are given in the supplementary material, Section S.6.

4. Conclusions

The (001), (011), and (111) surfaces of LZ are studied theoretically. A large set of defective (001) and (011) surface terminations is considered to complement a previous theoretical study of the LZ (001) and (011) surfaces [31], while the (111) surface of a compound in the large and important class of compounds known as the pyrochlore oxides is studied theoretically for the first time. All possible ideal surface terminations of the (001), (011), and (111) surfaces are examined, as well as several defective surface terminations of a surface. The expression for the surface free energy of a LZ surface is given, and surface energies and surface free energies are computed. The latter results are used to construct SPDs, which are shown not to depend strongly on vibrational contributions obtained from computed phonon dispersions.

From these SPDs, the main conclusions are drawn. First, only a few surface terminations of a given surface are identified as preferred out of the large set considered for the surface. In addition, the preferred surface termination of the (001), (011), or (111) surface is concluded to

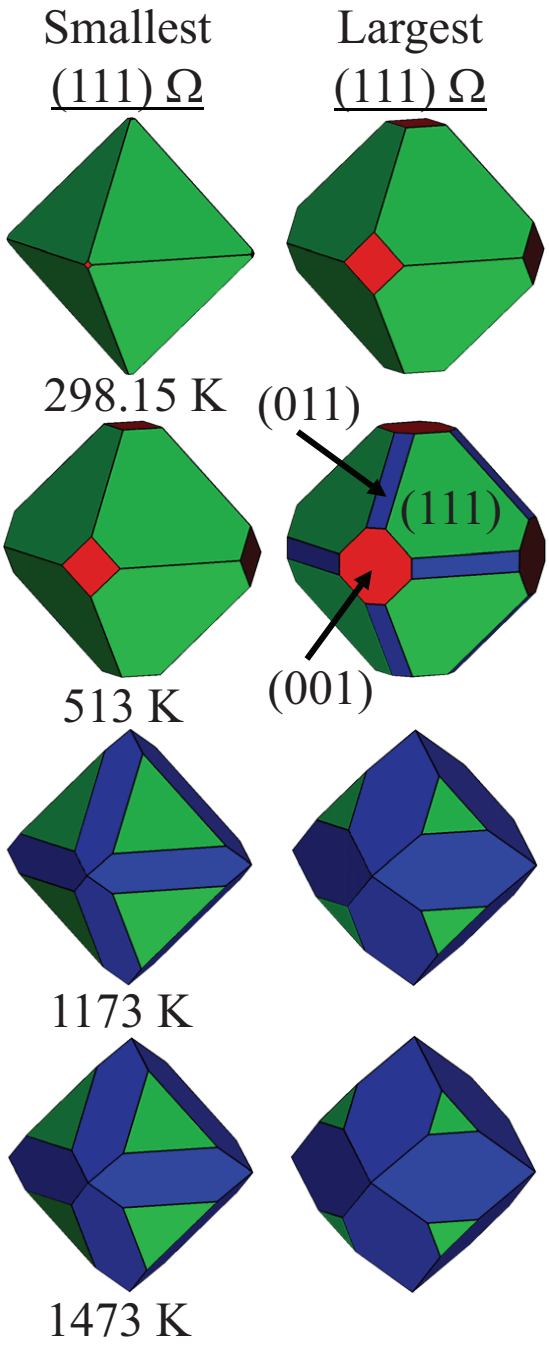

Figure 10: Wulff shapes of LZ based on preferred ideal surface terminations of the (001), (011), and (111) surfaces. They are made using Ω of the preferred ideal (001) and (011) surface terminations and the (left column) smallest and (right column) largest Ω of the preferred ideal (111) surface termination at 0.2 atm O_2 gas and (top row) 298.15 K, (second row) 513 K, (third row) 1173 K, and (bottom row) 1473 K.

be nonideal over a large set of T and p_{O_2} conditions. The different sets of conditions where the low-index surfaces are nonideal based on the SPDs are shown in Fig. 9. Lastly, a comparison to experiment is proposed, in which certain Wulff shapes are compared to experimental crystal shapes to provide some insight into the surface structures of the experimental shapes. However, more experimental work needs to be done to permit this comparison.

5. Acknowledgements

This work was funded by the SOFC program at the National Energy Technology Laboratory. This report was prepared as an account of work sponsored by an agency of the United States Government. Neither the United States Government nor any agency thereof, nor any of their employees, makes any warranty, express or implied, or assumes any legal liability or responsibility for the accuracy, completeness, or usefulness of any information, apparatus, product, or process disclosed, or represents that its use would not infringe privately owned rights. Reference therein to any specific commercial product, process, or service by trade name, trademark, manufacturer, or otherwise does not necessarily constitute or imply its endorsement, recommendation, or favoring by the United States Government or any agency thereof. The views and opinions of authors expressed therein do not necessarily state or reflect those of the United States Government or any agency thereof.

6. Supplementary material

Supplementary material associated with this article can be found in the online version.

7. Appendix

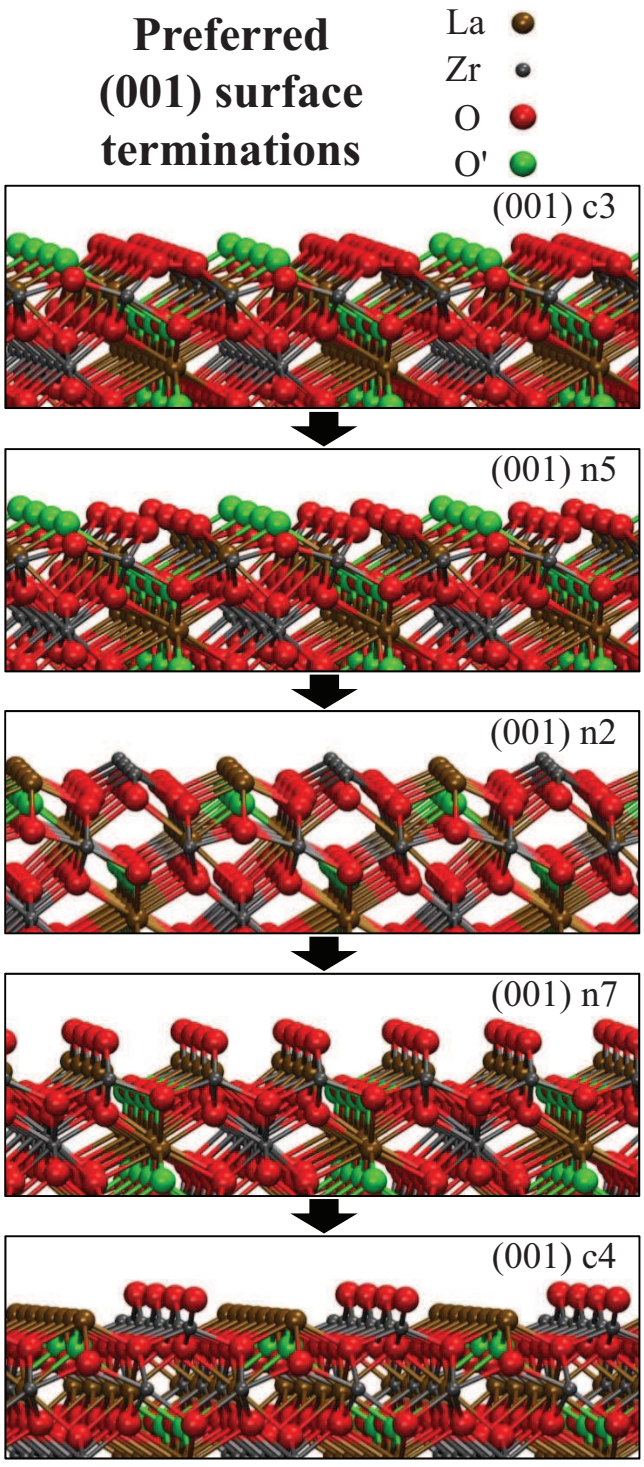

Figure A.1: Preferred relaxed (001) surface termination for decreasing $\Delta\mu_O$. Side views of 3 × 4 surface unit cell representations are shown.

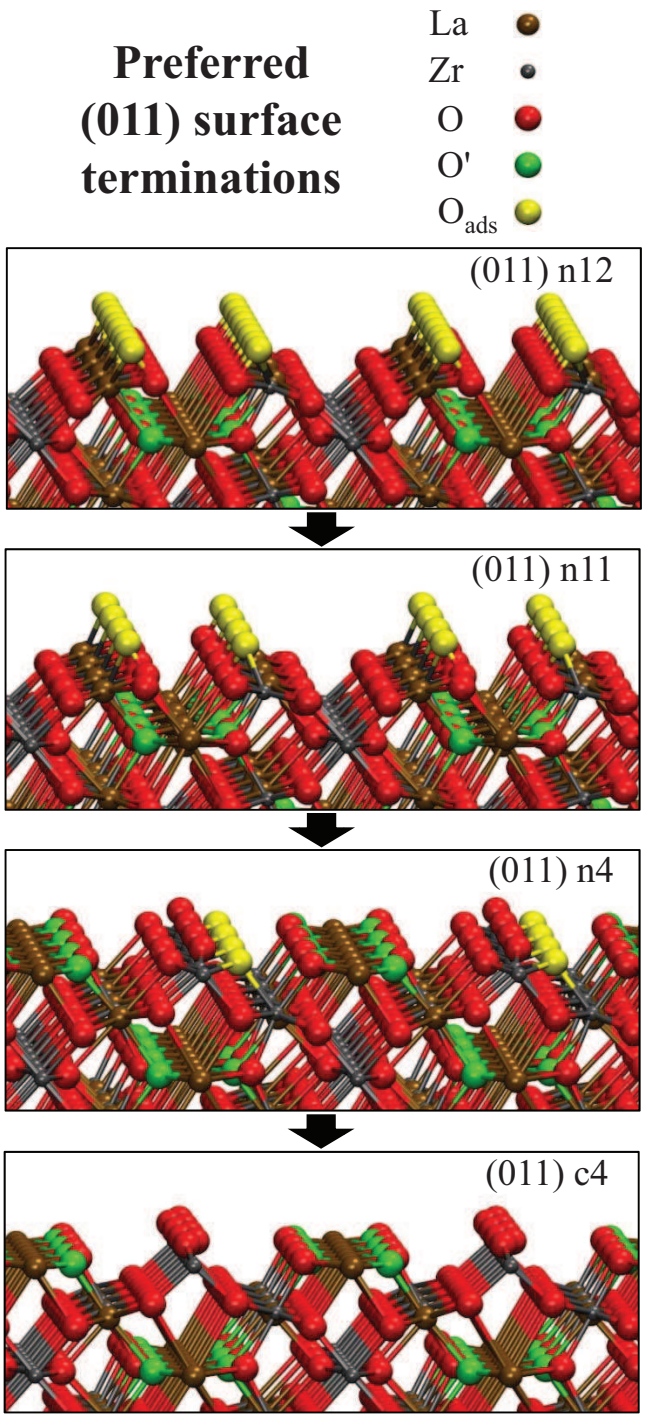

Figure A.2: Preferred relaxed (011) surface termination for decreasing $\Delta\mu_O$. Side views of 2 $\times$ 4 surface unit cell representations are shown.

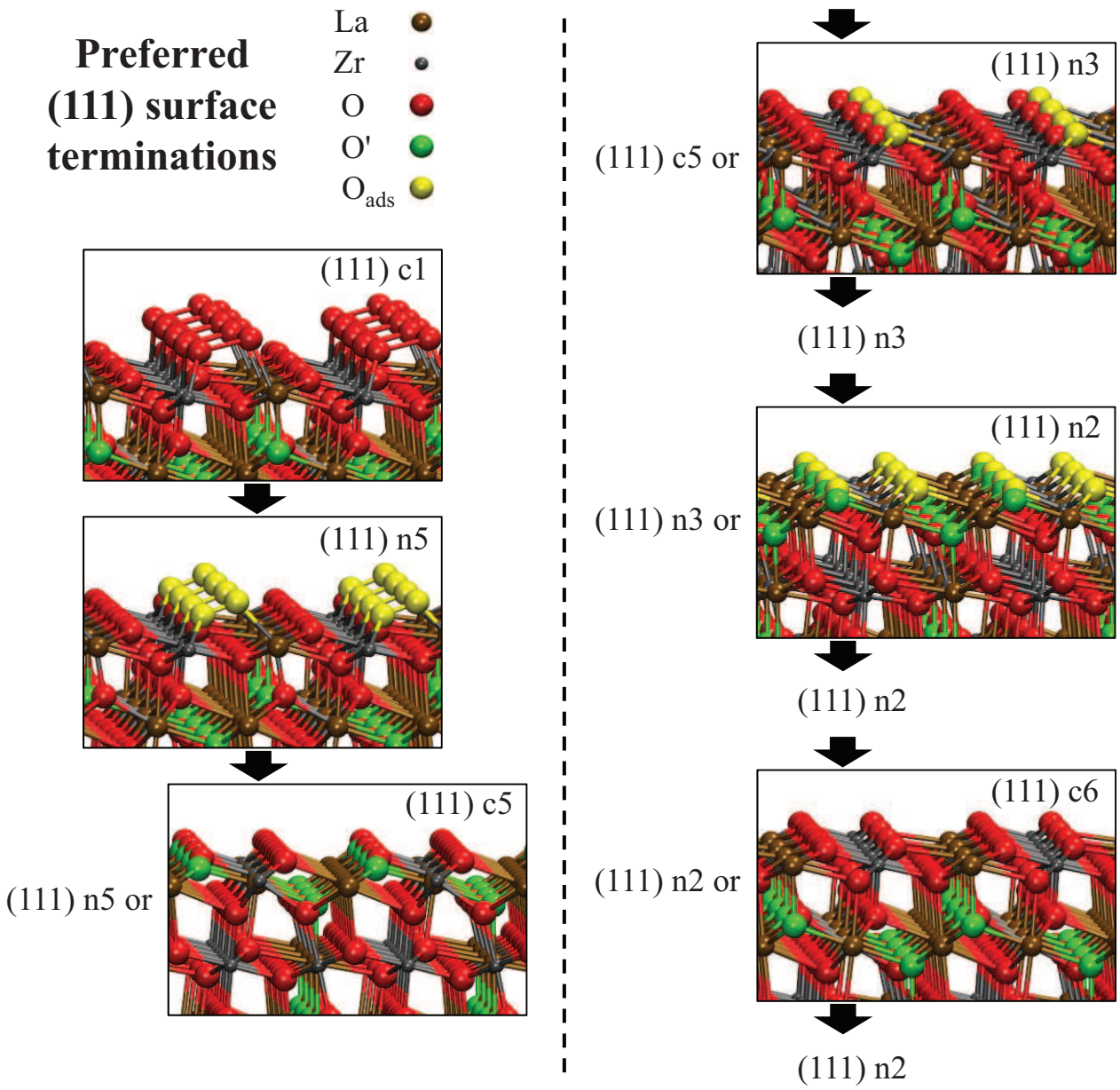

Figure A.3: Preferred relaxed (111) surface termination for decreasing $\Delta\mu_O$. Side views of 2 × 4 surface unit cell representations are shown.

References

[1] D. J. Haynes, D. A. Berry, D. Shekhawat, J. J. Spivey, Catalytic partial oxidation of n-tetradecane using pyrochlores: effect of Rh and Sr substitution, Catal. Today 136 (2008) 206–213.

[2] D. J. Haynes, D. A. Berry, D. Shekhawat, J. J. Spivey, Catalytic partial oxidation of n-tetradecane using Rh and Sr substituted pyrochlores: effects of sulfur, Catal. Today 145 (2009) 121–126.

[3] D. J. Haynes, A. Campos, D. A. Berry, D. Shekhawat, A. Roy, J. J. Spivey, Catalytic partial oxidation of a diesel surrogate fuel using an Ru-substituted pyrochlore, Catal. Today 155 (2010) 84–91.

[4] D. J. Haynes, A. Campos, M. W. Smith, D. A. Berry, D. Shekhawat, J. J. Spivey, Reducing the deactivation of Ni-metal during the catalytic partial oxidation of a surrogate diesel fuel mixture, Catal. Today 154 (2010) 210–216.

[5] M. W. Smith, D. Shekhawat, D. A. Berry, D. J. Haynes, D. L. Floyd, J. J. Spivey, O. Ranasingha, Carbon formation on Rh-substituted pyrochlore catalysts during partial oxidation of liquid hydrocarbons, Appl. Catal., A 502 (2015) 96–104.

[6] S. Gaur, D. J. Haynes, J. J. Spivey, Rh, Ni, and Ca substituted pyrochlore catalysts for dry reforming of methane, Appl. Catal., A 403 (2011) 142–151.

[7] S. Gaur, D. Pakhare, H. Wu, D. J. Haynes, J. J. Spivey, CO_2 reforming of CH_4 over Ru-substituted pyrochlore catalysts: effects of temperature and reactant feed ratio, Energy Fuels 26 (2012) 1989–1998.

[8] D. Pakhare, D. Haynes, D. Shekhawat, J. Spivey, Role of metal substitution in lanthanum zirconate pyrochlores ($La_2Zr_2O_7$) for dry (CO_2) reforming of methane (DRM), Appl. Petrochem. Res. 2 (2012) 27–35.

[9] D. Pakhare, H. Wu, S. Narendra, V. Abdelsayad, D. Haynes, D. Shekhawat, D. Berry, J. Spivey, Characterization and activity study of the Rh-substituted pyrochlores for CO_2 (dry) reforming of CH_4, Appl. Petrochem. Res. 3 (2013) 117–129.

[10] D. Pakhare, C. Shaw, D. Haynes, D. Shekhawat, J. Spivey, Effect of reaction temperature on activity of Pt- and Ru-substituted lanthanum zirconate pyrochlores ($La_2Zr_2O_7$) for dry (CO_2) reforming of methane (DRM), J. CO_2 Util. 1 (2013) 37–42.

[11] D. Pakhare, V. Schwartz, V. Abdelsayad, D. Haynes, D. Shekhawat, J. Poston, J. Spivey, Kinetic and mechanistic study of dry (CO_2) reforming of methane over Rh-substituted $La_2Zr_2O_7$ pyrochlores, J. Catal. 316 (2014) 78–92.

[12] F. Polo-Garzon, M. He, D. A. Bruce, *Ab initio* derived reaction mechanism for the dry reforming of methane on Rh doped pyrochlore catalysts, J. Catal. 333 (2016) 59–70.

[13] F. Polo-Garzon, D. Pakhare, J. J. Spivey, D. A. Bruce, Dry reforming of methane on Rh-doped pyrochlore catalysts: a steady-state isotopic transient kinetic study, ACS Catal. 6 (2016) 3826–3833.

[14] F. Polo-Garzon, J. K. Scott, D. A. Bruce, Microkinetic model for the dry reforming of methane on Rh doped pyrochlore catalysts, J. Catal. 340 (2016) 196–204.

[15] N. Kumar, A. Roy, Z. Wang, E. M. L'Abbate, D. Haynes, D. Shekhawat, J. J. Spivey, Bi-reforming of methane on Ni-based pyrochlore catalyst, Appl. Catal., A 517 (2016) 211–216.

[16] N. Kumar, Z. Wang, S. Kanitkar, J. J. Spivey, Methane reforming over Ni-based pyrochlore catalyst: deactivation studies for different reactions, Appl. Petrochem. Res. 6 (2016) 201–207.

[17] J. Cheng, J. Li, C. Ma, Z. Hao, Catalytic combustion of methane over $La_2TM_{0.3}Zr_{1.7}O_{7-\delta}$ (TM = Mn, Fe, and Co) pyrochlore oxides, Catal. Commun. 10 (2009) 1170–1173.

[18] V. Abdelsayad, D. Shekhawat, J. Poston, James A., J. J. Spivey, Synthesis, characterization, and catalytic activity of Rh-based lanthanum zirconate pyrochlores for higher alcohol synthesis, Catal. Today 207 (2013) 65–73.

[19] S. Lee, N. Miller, H. Abernathy, K. Gerdes, A. Manivannan, Effect of Sr-doped $LaCoO_3$

and $LaZrO_3$ infiltration on the performance of SDC-LSCF cathode, J. Electrochem. Soc. 158 (2011) B735–B742.

[20] M. A. Subramanian, G. Aravamudan, G. V. Subba Rao, Oxide pyrochlores – a review, Prog. Solid State Chem. 15 (1983) 55–143.

[21] Y. Tabira, R. L. Withers, L. Minervini, R. W. Grimes, Systematic structural change in selected rare earth oxide pyrochlores as determined by wide-angle CBED and a comparison with the results of atomistic computer simulation, J. Solid State Chem. 153 (2000) 16–25.

[22] Y. Tong, J. Zhu, L. Lu, X. Wang, X. Yang, Preparation and characterization of $Ln_2Zr_2O_7$ (Ln = La and Nd) nanocrystals and their photocatalytic properties, J. Alloys Compd. 465 (2008) 280–284.

[23] K. Koteswara Rao, T. Banu, M. Vithal, G. Swamy, K. Ravi Kumar, Preparation and characterization of bulk and nano particles of $La_2Zr_2O_7$ and $Nd_2Zr_2O_7$ by sol-gel method, Mater. Lett. 54 (2002) 205–210.

[24] A. K. Bhattacharya, A. Hartridge, K. K. Mallick, J. L. Woodhead, Preparation and characterization of $Ln_2Zr_2O_7$ microspheres by an inorganic sol-gel route, J. Mater. Sci. 29 (1994) 6076–6078.

[25] D. Chen, R. Xu, Hydrothermal synthesis and characterization of $La_2M_2O_7$ (M = Ti, Zr) powders, Mater. Res. Bull. 33 (1998) 409–417.

[26] H. Zhou, D. Yi, Z. Yu, L. Xiao, Preparation and thermophysical properties of CeO_2 doped $La_2Zr_2O_7$ ceramic for thermal barrier coatings, J. Alloys Compd. 438 (2007) 217–221.

[27] J. W. Seo, J. Fompeyrine, A. Guiller, G. Norga, C. Marchiori, H. Siegwart, J.-P. Locquet, Interface formation and defect structures in epitaxial $La_2Zr_2O_7$ thin films on (111) Si, Appl. Phys. Lett. 83 (2003) 5211–5213.

[28] H. S. Chen, R. V. Kumar, B. A. Glowacki, Chemical solution deposited lanthanum

zirconium oxide thin films: synthesis and chemistry, Mater. Chem. Phys. 122 (2010) 305–310.

[29] Y. A. Mantz, Defect-free and defective surfaces of the pyrochlore oxide $La_2Zr_2O_7$: a theoretical study, in: S.-H. Wei, A. Rubio, H. Guo, L. Liu (Eds.), 2011 MRS Spring Meeting - Volume 1370 - Symposium YY – Computational Semiconductor Materials Science, Cambridge University Press, Cambridge, 2011. http://dx.doi.org/10.1557/opl.2011.1041 (accessed 2017).

[30] Y. A. Mantz, Surface properties, crystal morphology, and reactivity of $La_2Zr_2O_7$-based cathode infiltrate in solid oxide fuel cells: a theoretical study, in: J. D. Perkins, A. Ohtomo, H. N. Lee, G. Herranz (Eds.), 2011 MRS Spring Meeting - Volume 1327 - Symposium G – Complex Oxide Materials for Emerging Energy Technologies, Cambridge University Press: Cambridge, 2011. http://dx.doi.org/10.1557/opl.2011.1259 (accessed 2017).

[31] Y. A. Mantz, Density-functional study of the $La_2Zr_2O_7$ (001) and (011) surfaces and bulk, J. Phys. Chem. C 120 (2016) 7522–7531.

[32] J. P. Perdew, J. A. Chevary, S. H. Vosko, K. A. Jackson, M. R. Pederson, D. J. Singh, C. Fiolhais, Atoms, molecules, solids, and surfaces: applications of the generalized gradient approximation for exchange and correlation, Phys. Rev. B: Condens. Matter Mater. Phys. 46 (1992) 6671–6687.

[33] J. P. Perdew, J. A. Chevary, S. H. Vosko, K. A. Jackson, M. R. Pederson, D. J. Singh, C. Fiolhais, Erratum: atoms, molecules, solids, and surfaces: applications of the generalized gradient approximation for exchange and correlation [Phys. Rev. B 46, 6671 (1992)], Phys. Rev. B: Condens. Matter Mater. Phys. 48 (1993) 4978.

[34] P. E. Blöchl, Projector augmented-wave method, Phys. Rev. B: Condens. Matter Mater. Phys. 50 (1994) 17953–17979.

[35] G. Kresse, D. Joubert, From ultrasoft pseudopotentials to the projector augmented-wave method, Phys. Rev. B: Condens. Matter Mater. Phys. 59 (1999) 1758–1775.

[36] VASP the Guide. http://cms.mpi.univie.ac.at/vasp/vasp (accessed 2017).

[37] E. A. Kotomin, R. A. Evarestov, Y. A. Mastrikov, J. Maier, DFT plane wave calculations of the atomic and electronic structure of $LaMnO_3$ (001) surface, Phys. Chem. Chem. Phys. 7 (2005) 2346–2350.

[38] H. J. Monkhorst, J. D. Pack, Special points for brillouin-zone integrations, Phys. Rev. B: Solid State 13 (1976) 5188–5192.

[39] J. P. Perdew, A. Zunger, Self-interaction correction to density-functional approximations for many-electron systems, Phys. Rev. B: Condens. Matter Mater. Phys. 23 (1981) 5048–5079.

[40] G. Kresse, J. Hafner, *Ab initio* molecular dynamics for liquid metals, Phys. Rev. B: Condens. Matter Mater. Phys. 47 (1993) 558–561.

[41] G. Kresse, J. Hafner, *Ab initio* molecular-dynamics simulation of the liquid-metal–amorphous-semiconductor transition in germanium, Phys. Rev. B: Condens. Matter Mater. Phys. 49 (1994) 14251–14269.

[42] G. Kresse, J. Furthmüller, Efficiency of ab-initio total energy calculations for metals and semiconductors using a plane-wave basis set, Comput. Mater. Sci. 6 (1996) 15–50.

[43] G. Kresse, J. Furthmüller, Efficient iterative schemes for *ab initio* total-energy calculations using a plane-wave basis set, Phys. Rev. B: Condens. Matter Mater. Phys. 54 (1996) 11169–11186.

[44] K. Parlinski, Software PHONON. http://wolf.ifj.edu.pl/phonon (accessed 2017), http://www.computingformaterials.com (accessed 2017).

[45] Dassault Systèmes BIOVIA, BIOVIA Materials Studio. http://accelrys.com/products/collaborative-science/biovia-materials-studio (accessed 2017).

[46] W. Humphrey, A. Dalke, K. Schulten, VMD – visual molecular dynamics, J. Molec. Graphics 14, (1996) 33–38. http://www.ks.uiuc.edu/Research/vmd (accessed 2017).

[47] R. Edwin García, J. Blendell, Equilibrium Wulff shape generator. http://nanohub.org/resources/wulffman (accessed 2017).

[48] D. R. Lide (Ed.), CRC Handbook of Chemistry and Physics, 72nd ed., CRC Press, Boca Raton, FL, 1991.

[49] K. Johnston, M. R. Castell, A. T. Paxton, M. W. Finnis, $SrTiO_3(001)(2\times1)$ reconstructions: first-principles calculations of surface energy and atomic structure compared with scanning tunneling microscopy images, Phys. Rev. B: Condens. Matter Mater. Phys. 70 (2004) 085415.

[50] L. Yang, Y. Jiang, G. R. Odette, W. Zhou, Z. Liu, Y. Liu, Nonstoichiometry and relative stabilities of $Y_2Ti_2O_7$ polar surfaces: a density functional theory prediction, Acta Mater. 61 (2013) 7260–7270.

[51] I. Schnell, M. D. Jones, S. P. Rudin, R. C. Albers, Tight-binding calculations of the elastic constants and phonons of hcp Zr: complications due to anisotropic stress and long-range forces, Phys. Rev. B: Condens. Matter Mater. Phys. 74 (2006) 054104.

[52] G. Fadda, G. Zanzotto, L. Colombo, First-principles study of the effect of pressure on the five zirconia polymorphs. I. Structural, vibrational, and thermoelastic properties, Phys. Rev. B: Condens. Matter Mater. Phys. 82 (2010) 064105.

[53] M. Sternik, K. Parlinski, Lattice vibrations in cubic, tetragonal, and monoclinic phases of ZrO_2, J. Chem. Phys. 122 (2005) 064707.

[54] A. Kuwabara, T. Tohei, T. Yamamoto, I. Tanaka, *Ab initio* lattice dynamics and phase transformations of ZrO_2, Phys. Rev. B: Condens. Matter Mater. Phys. 71 (2005) 064301.

[55] G. P. Cousland, X. Y. Cui, S. Ringer, A. E. Smith, A. P. J. Stampfl, C. M. Stampfl, Electronic and vibrational properties of yttria-stabilised zirconia from first-principles for $10-40$ mol% Y_2O_3, J. Phys. Chem. Solids 75 (2014) 1252–1264.

[56] S. Bağcı, H. M. Tütüncü, S. Duman, G. P. Srivastava, Phonons and superconductivity in fcc and dhcp lanthanum, Phys. Rev. B: Condens. Matter Mater. Phys. 81 (2010) 144507.

[57] C. Wang, O. Fabrichnaya, M. Zinkevich, Y. Du, F. Aldinger, Experimental study and thermodynamic modelling of the ZrO_2–$LaO_{1.5}$ system, CALPHAD: Comput. Coupling Phase Diagrams Thermochem. 32 (2008) 111–120.

[58] E. A. Ahmad, L. Liborio, D. Kramer, G. Mallia, A. R. Kucernak, N. M. Harrison, Thermodynamic stability of $LaMnO_3$ and its competing oxides: a hybrid density functional study of an alkaline fuel cell catalyst, Phys. Rev. B: Condens. Matter Mater. Phys. 84 (2011) 085137.

[59] A. V. Radha, S. V. Ushakov, A. Navrotsky, Thermochemistry of lanthanum zirconate pyrochlore, J. Mater. Res. 24 (2009) 3350–3357.

[60] L. Wang, T. Maxisch, G. Ceder, Oxidation energies of transition metal oxides within the GGA+U framework, Phys. Rev. B: Condens. Matter Mater. Phys. 73 (2006) 195107.

[61] Y.-L. Lee, J. Kleis, J. Rossmeisl, D. Morgan, *Ab initio* energetics of LaBO$_3$(001) (B = Mn, Fe, Co, and Ni) for solid oxide fuel cell cathodes, Phys. Rev. B: Condens. Matter Mater. Phys. 80 (2009) 224101.

[62] F. Bottin, F. Finocchi, C. Noguera, Stability and electronic structure of the (1×1) $SrTiO_3$(110) polar surfaces by first-principles calculations, Phys. Rev. B: Condens. Matter Mater. Phys. 68 (2003) 035418.

[63] E. Heifets, J. Ho, B. Merinov, Density functional simulation of the $BaZrO_3$ (011) surface structure, Phys. Rev. B: Condens. Matter Mater. Phys. 75 (2007) 155431.

[64] Yu. A. Mastrikov, E. Heifets, E. A. Kotomin, J. Maier, Atomic, electronic and thermodynamic properties of cubic and orthorhombic $LaMnO_3$ surfaces, Surf. Sci. 603 (2009) 326–335.

[65] C.-W. Lee, R. K. Behera, E. D. Wachsman, S. R. Phillpot, S. B. Sinnott, Stoichiometry of the $LaFeO_3$ (010) surface determined from first-principles and thermodynamic calculations, Phys. Rev. B: Condens. Matter Mater. Phys. 83 (2011) 115418.

[66] D. Sherwood, B. Emmanuel, Computing shapes of nanocrystals from X-ray diffraction data, Cryst. Growth Des. 6 (2006) 1415–1419.

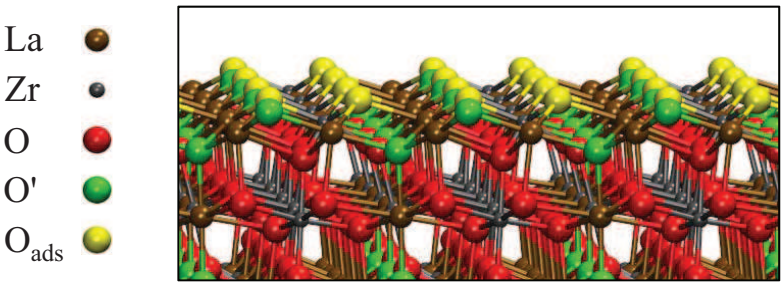

Figure 11: Graphical abstract